A probabilistic model for coseismic vertical displacement hazard in coastal settings

Jaime Delano[1], Andy Howell [1,2], Kate Clark[2], Tim Stahl[1], Chris Rollins[2], Hannu Seebeck[2], and Jack McGrath[1]

[1]*School of Earth and Environment, Te Whare Wānanga o Waitaha | University of Canterbury, Christchurch, Aotearoa New Zealand*

[2] *Te Pū Ao | GNS Science, Lower Hutt, Aotearoa New Zealand*

ABSTRACT

Characterizing coastal multi-hazards in tectonically active regions requires considering possible coseismic vertical deformation. Coseismic uplift or subsidence can cause near-instantaneous meter-scale relative sea level changes that can exacerbate or reverse the effects of ongoing global sea-level rise. In this study, we developed a probabilistic model that forecasts coseismic vertical displacement over 100 years in the Wellington Region of Aotearoa New Zealand. This model repurposes fault source, earthquake rupture, and epistemic uncertainty data from the New Zealand National Seismic Hazard Model (NZ NSHM 2022) to quantify the amount, direction, and likelihood of vertical displacement from both crustal fault and subduction interface earthquakes. The results of the model show that both crustal fault and subduction sources pose significant (>0.2 m) vertical displacement hazard at most sites. In general, the subduction interface contributes more to subsidence hazard, while crustal faults contribute more to uplift hazard but also contribute to subsidence hazard at specific sites. We find that fault geometry and slip extent plays a significant role in forecasted uplift and subsidence hazard; future versions of both the NZ NSHM 2022 and this model may benefit from refinements to fault geometry and simulated earthquake ruptures. The framework developed here can be used to harness regional scale hazard models for coastal multi-hazard analysis, particularly in regions with many overlapping seismic sources.

1. INTRODUCTION

Hazard models and forecasts are useful for understanding the likelihood of earthquake effects and inform mitigation strategies, engineering standards, and resilience plans (e.g., Silva et al., 2023). For example, buildings and infrastructure may be built to withstand certain intensities of forecasted ground motions (e.g., Heintz et al., 2022) or large displacements along mapped fault traces (e.g., Youngs et al., 2003; International Atomic Energy Agency, 2021). Tsunami hazard models are used to inform land-use planning and evacuation routes (e.g., United Nations Office for Disaster Risk Reduction, 2017). These forecasts provide site-specific hazard estimates that guide decision-making processes.

Sea-level change forecasts, based on the combined effects of climate-induced sea0-level rise and continuous tectonic vertical land motions (VLMs), are increasingly considered in coastal hazard and resilience planning (e.g., Ministry for the Environment, 2024). At present, these forecasts do not typically include the sudden, coseismic VLMs from earthquakes (e.g., Ministry for the Environment, 2024). Coastal regions are particularly vulnerable to multi-hazards because relative sea level changes can reduce or exacerbate flooding, tsunami, storm surges, and erosion; alter coastal ecosystems; and decrease functionality of critical infrastructure (Fig. 1). Coseismic VLMs happen infrequently but the magnitude (up to several meters) (Fig. 1) can greatly exceed comparatively smaller amounts of continuous deformation from other processes (e.g., millimeters per year from sediment compaction) (Hamling et al., 2022). This stochastic behavior of earthquakes presents challenges for hazard planning because the likelihood of coseismic VLM is low over human and city-development time scales (~50–100 years) but the potential impacts are large. In particular, adaptations to projected global sea-level rise over the next century may be thwarted or made redundant by coseismic VLMs. Quantifying the probabilities of different amounts of coseismic deformation from different fault sources is thus a key component of developing a full picture of coastal hazards over the next 100 years.

Aotearoa New Zealand is an island nation situated along a major tectonic plate boundary (Fig. 2); thus, much of the population, places of cultural significance, and critical infrastructure is both near the coast and in regions with significant earthquake hazards. Advances in paleoearthquake and fault source characterization research has allowed for detailed seismic hazard models that define engineering standards. The New Zealand National Seismic Hazard Model–Te Tauira Matapae Pūmate Rū i Aotearoa (NZ NSHM 2022) forecasts ground shaking for the next 100 years of earthquakes and represents a fundamental and significant revision based on the last two decades of research and technological improvements (Gerstenberger et al., 2022a, 2024a). These new data and modelling tools present an opportunity to estimate how Aotearoa New Zealand's coasts may vertically deform over 100 years of earthquakes.

In this study we seek to develop the first probabilistic coseismic displacement hazard model (PCDHM) based on a national seismic hazard dataset that focuses on coastal vertical deformation in the Wellington Region, Aotearoa New Zealand. This region occupies a complex tectonic setting that is susceptible to earthquake hazards from both the Hikurangi subduction interface and upper plate crustal faults (henceforth we use "crustal faults"). Additionally, it hosts the capital city Wellington, one of the largest and densest population centers in Aotearoa New Zealand and the locus of Aotearoa New Zealand's seismic risk (Silva et al., 2023). The aim is to use the data and results from the NZ NSHM 2022, including earthquake ruptures and annual rates of occurrence, to calculate coastal coseismic displacements and associated probabilities. The results provide a means of comparing the magnitude and frequency of expected vertical coseismic displacement hazards at different sites and the relative contributions from the subduction interface and crustal fault sources. This work lays a foundation for additional probabilistic models and hazard analyses globally such as coseismic vertical deformation inland, horizontal displacement hazards, and site-specific multi-hazard analyses.

2. BACKGROUND

2.1 Tectonic Setting

Aotearoa New Zealand is situated along the Pacific-Australian plate boundary (Fig. 2A, inset). Beneath the southern North Island, toward the southern termination of the Hikurangi Subduction zone, the Pacific plate subducts westward beneath the Australian plate. Here, the c. 40 mm/yr oblique relative plate motion is partitioned between the subduction interface (~80%) and upper plate faults (~20%) (Fig. 2) (Beavan et al., 2002; Nicol and Beavan, 2003). Obliquity between relative plate convergence vector and the plate boundary strike increases southward along the Hukurangi subduction zone (Wallace et al., 2004; Wallace, 2020). As a result, upper plate faults accommodate a higher portion of relative plate motion near the southern Hikurangi subduction zone (Wallace et al., 2004; Nicol and Wallace, 2007).

The Wellington Region occupies this transitional zone where significant plate motion is transferred from the subduction interface to upper plate faults (Fig. 2). Closer to the Hikurangi trench along the eastern side of the Wellington Region are a series of imbricate gently dipping or listric reverse forearc faults (Beanland and Haines, 1998). Westwards, the North Island Dextral Fault System (NIDFS) mainly accommodates margin-parallel motion from oblique convergence of the southern Hikurangi subduction zone (e.g., Litchfield et al., 2014). Faults in the NIDFS generally have steep dips in the near-surface but at depth the fault geometries are more difficult to determine (e.g., Little et al., 2009). Interpretations of active source seismic data that transect the Wellington Region indicate a complex interaction between upper plate faults, underplated sediments, and the subduction interface (Henrys et al., 2013). Here, geometric uncertainty of fault dip and down-dip extent stems from the difficulty imaging a dense and complex arrangement of faults compounded by heterogeneous crustal properties (Henrys et al., 2013). The most recent subsurface interpretations in this region suggest the upper plate faults may have much gentler dips at depth than the surface and merge with a network of thrust duplexes within underplated sediments above the subduction interface (Henrys et al., 2013).

One surface-rupturing earthquake, the 1855 M_w 8.2 Wairarapa earthquake, has occurred in the Wellington Region since European arrival at c. 1840 C.E (Darby and Beanland, 1992; Little and Rodgers, 2005). Geological observations and subsequent modelling suggest that this event occurred on the Wairarapa Fault and Wharekauhau Thrust (Fig. 2) (Beavan and Darby, 2005). The event produced widespread meter-scale uplift west of Palliser Bay, with peak uplift of 6.4 m near Turakirae Head tapering to c. 0.3-1.0 m uplift near Porirua (Grapes and Downes, 1997; King et al., 2024). This surface deformation suggests a more gently dipping fault than is exposed at the surface; and may have included slip on the subduction interface (Beavan and Darby, 2005). The coseismic uplift significantly altered the coastline by widening beaches, uplifting rocky reefs, draining coastal marshes, and facilitating further development of Wellington city and nearby towns (Grapes and Downes, 1997).

2.2 The NZ NSHM 2022

The computational approach used in this study incorporates preexisting frameworks developed for other probabilistic and earthquake deformation studies (i.e. the NZ NSHM 2022); at times, their respective terminologies can sound similar and are confusing to describe out of their original context. We provide a glossary of terms (Table 1) to clarify different types of models, model components, specific terminology and initialisms adopted for this study, and terms common in the earthquake and natural hazards space.

The approach for making this PCDHM follows similar principles to a probabilistic seismic hazard assessment (PSHA). A PSHA quantifies the liklihood of exceeding ground motion thresholds at specific sites from all possible earthquakes over a specified time interval (e.g., Cornell, 1968; Budnitz et al., 1997). A probabilistic approach is useful because strong ground motions and large displacements occur less frequently (i.e., from large magnitude close earthquakes) compared to more frequent weak ground motions and small displacements (i.e., smaller magnitude and/or distal earthquakes). PSHA products provide a framework for decision makers based on both the risks different ground motions pose and their likelihood (e.g., Field et al., 2017; Gerstenberger et al., 2022a, 2024a).

This PCDHM study incorporates the Seismicity Rate Model (SRM) from the 2022 NZ NSHM 2022, a national-scale PSHA (Gerstenberger et al., 2022a, 2024a). We summarize below the primary components of the SRM that are included, omitted, or modified for this study.

The SRM defines the fault sources, earthquake rupture scenarios, and logic tree used in the NZ NSHM 2022. The SRM includes the Inversion Fault Model (IFM), which is based on defined fault sources, as well as the Distributed Seismicity Model (DSM), which captures earthquakes from currently unknown faults (Gerstenberger et al., 2022a, 2024a). We omitted the

DSM from this study because it primarily models smaller earthquakes unlikely to cause VLM >0.1-0.2 m, and the fault network in the Wellington Region is generally well-constrained by seismic survey data. However, future studies should investigate the sensitivity of models to distributed seismicity, especially since mm-to-cm coseismic VLM could bias measurements of interseismic VLM.

The SRM includes two fault source types: subduction interfaces and crustal faults. We include the Hikurangi interface and exclude the Puysegur subduction zone, which is too far away to cause impactful displacement in the Wellington Region. The crustal fault sources are based on the Community Fault Model (CFM), a simplified fault network of mostly planar fault segments (Seebeck et al., 2022).

For each fault source type (i.e., crustal or subduction), the SRM includes a weighted-branch logic tree to quantify epistemic uncertainties (Gerstenberger et al., 2022b, 2024b). All SRM branches include a suite of hundreds of thousands of synthetic earthquake rupture scenarios. The solutions for each branch comprise average slip and an annual rate of occurrence per rupture scenario (Gerstenberger et al., 2022b, 2024b).

Probabilistic displacements estimated in this study incorporate the crustal fault network, rupture scenarios, earthquake scenario solutions (annual rates and average slip values), and branch weights from the SRM. In some instances, we included additional modified fault models as described in subsequent sections. Further information on branch parameters and solutions can be found in the NZ NSHM 2022 documentation and references within (Gerstenberger et al., 2022a, 2024a).

3. METHODS

3.1 Approach

The primary stages involved in creating this PCDHM include (i) calculating coseismic surface displacements at targeted sites from individual earthquakes ruptures, (ii) capturing a range of possible earthquake displacements in 100-yr periods based on the NZ NSHM 2022 solutions, and (iii) calculating the probabilities of exceeding vertical displacement values at targeted sites (Fig. 3).

The SRM provides a framework for this PCDHM to calculate coseismic displacements and probabilities, as well as quantify many epistemic uncertainties (Fig. 3). However, because the NZ NSHM 2022 was developed for a different purpose (ground motion hazard), some components must be altered or recognized as a limitation in this PCDHM.

There are several key differences between a ground motion and vertical displacement hazards (and thus a PSHA and a PCDHM). First, over a specified time period (e.g., 100 years), repeated coseismic vertical deformation is cumulative, whereas ground motions are transient and return to zero between earthquakes. Therefore, vertical changes at the coast can reduce or enhance the effects of subsequent events. A standard PSHA approach, when applied to displacement hazard, would address the question: What are the probabilities of exceeding a single coseismic displacement value from all seismic sources in a 100-year interval? Instead, a more apt question is: What are the probabilities of exceeding a cumulative displacement value for all earthquakes that occur within a 100-year interval? Or, from a design and mitigation perspective, what cumulative displacement values should be prepared for, given displacement probabilities from all possible earthquakes?

Additionally, in contrast with peak ground motion accelerations, vertical coseismic displacements can be up or down (i.e., uplift or subsidence). Repeated vertical displacements in the same direction produce larger net displacements than multiple displacements in opposite directions. Further, the impact of coseismic coastal uplift versus subsidence vary greatly (Fig. 1). Therefore, both the displacement direction and magnitude must be considered for probabilistic displacement hazard models.

We describe details of our approach below; full details and scripts are available in the accompanying data repository (Delano et al., 2024).

3.2 Fault Meshes and Geometries

The catalogue of earthquake ruptures and associated annual rates from the SRM (Gerstenberger et al., 2022a, 2024a) is a key component of this PCDHM. The rupture scenarios provided a basis for calculating surface displacements for hypothetical earthquakes (step 2 in Fig. 3), while the annual rates underpin the probability calculations (step 3 in Fig. 3). Both are based on the best-available published data such as slip rates, fault geometry, past earthquake slip behavior, geodetic and geologic strain, and magnitude scaling relationships (Gerstenberger et al., 2022b, 2024b).

The SRM divides each fault source into smaller planar ‘subsections’ to facilitate calculating seismic hazard. Each crustal or subduction interface earthquake rupture scenario consists of a collection of subsections, an associated average slip, and an annual rate of occurrence. Heavily modifying any of these components (slip, annual rate, fault network, rupture extent) would likely necessitate a new inversion and ultimately alter the solution rates. For simplicity, we opted to repurpose the SRM data and solutions. Small changes in geometry, such as fault dip angle or slip rake, are potentially permissible to evaluate how these parameters influence the final displacement hazard but may also have broad scale implications to the slip and deformation budget. We have not assessed the influence of alternative fault geometries on the SRM solutions.

We modified the planar SRM fault subsections into a continuous, discretized triangular meshes for this PCDHM. This eliminated spatial gaps or overlapping intersections between adjacent fault subsections which reduced unrealistic surface deformation patterns. We also tested several alternative fault geometries for crustal fault sources (expanded below) (Step 1, Fig. 3). Crustal fault dips in the CFM are typically based on near-surface data and do not take into account decreasing dip angle with depth (e.g., Bray et al., 1994; Barnes et al., 2002; Amos et al., 2007; Henrys et al., 2013). Changes in average fault dip influence both the modelled vertical deformation pattern and displacement hazards (Okada, 1985).

The Hikurangi subduction interface mesh geometry and rake are from Williams et al. (2013) and Wallace et al. (2009), respectively. We approximated the surface with triangles of side length ~3 km, which gives a smooth representation of the geometry while also allowing rapid calculation of surface deformation. To test how interface depth uncertainty affected displacements, we calculated displacements on three subduction interface meshes: one that follows the Williams et al. (2013) geometry with no modifications, one with a steeper overall interface dip, and one with an overall gentler dip. The steeper and gentler dip interface meshes were created by multiplying the depth coordinate of the mesh vertices by 1.15 and 0.85, respectively.

For simplicity, the entire set of triangular crustal fault surfaces are referred to here as a single crustal fault "mesh." We calculated displacements on three crustal meshes to test fault geometry sensitivity: the CFM Mesh, Alternative Fault 1 Mesh (Alt. Fault 1 Mesh), and Alternative Fault 2 Mesh (Alt. Fault 2 Mesh) (Table S1). All the meshes used in this study are truncated at the Wellington Region boundary in the north and on the southern side of Cook Strait in the south and discretized using a triangle edge length of 2 km using Coreform Cubit software (Fig. 1).

The CFM Mesh uses the 'preferred' value for dip and rake in the CFM (and as used in the SRM; Seebeck et al., 2022) (Fig. 2c). The alternative fault mesh geometries below were based on expert advice from members of the NZ NSHM 2022 working group (Van Dissen et al., 2023).

Alt. Fault 1 Mesh is the same as the CFM mesh except for vertical pure strike-slip faults; these structures are changed to 80° SE-dipping faults with a minor normal component (rake of -160°) (Fig. 2C, Table S1). These dip and rake variations are within maximum or minimum values in the published CFM (Seebeck et al., 2022). They test how small changes in fault dip and rake, as induced by fault steps and bends, might affect surface deformation, and are consistent with potential normal fault slip as observed in seismic survey data near the Kapiti Coast (Lamarche et al., 2005).

The Alt. Fault 2 Mesh deviates more from the CFM and covers additional plausible fault geometries throughout the Wellington Region (Fig. 2C, Table S1). First, as a correlate to Alt. Fault Mesh 1, we imposed a 80° NW dip and small component of reverse slip (rake +160°) to any vertical pure strike-slip fault in the CFM. Next, we reduced the dip angle on most of the reverse faults east of Wellington city. For some structures, these modified dip values are lower than the minimum dip in the CFM (Seebeck et al., 2022). Our selected dips are consistent with low-angle, listric crustal geometry from seismic imaging and recent elastic dislocation model results for fault-controlled marine terrace uplift (Henrys et al., 2013; Ninis et al., 2023). Finally, some of the offshore crustal faults northwest of the Wellington Region may be backthrusts to the subduction interface that dip southeast (Lamarche et al., 2005); we include this possible geometry in the western offshore faults of Alt. Fault Mesh 2.

The Palliser-Kaiwhata fault is ~20 km longer in Alt. Fault Mesh 1 and 2 than the CFM Mesh. This reverse structure likely contributes to long-term uplift at Cape Pallier (Ninis et al., 2023), but in the CFM, the fault surface does not underlie Cape Palliser (see dashed fault trace in Fig. 2C) (Seebeck et al., 2022). The longer length in the Alt. Fault 1 and 2 Meshes ensure that earthquakes on that structure can displace the coastline at Cape Palliser (Fig. 2B).

Neither the CFM mesh, Alt. Fault 1 or Alt. Fault 2 Mesh are necessarily more correct than the others, but they provide a means of determining how uncertainties or simplifications in fault and slip geometry might impact displacement hazard estimates.

All meshes used in the elastic dislocation models were discretized into groups based on the closest SRM fault subsection centroid to facilitate using the SRM rupture sets. For the Hikurangi subduction mesh, fault subsections were assigned by a combination of map distance and depth coordinate (Fig. S1).

3.3 Elastic Dislocation Modelling

Elastic dislocation models are a tool to calculate coseismic displacement from specified slip on a fault surface. We used the six above fault meshes (subduction interface-no modifications, subduction interface-steeper dip, subduction interface-gentler dip, CFM Mesh, Alt. Fault 1 Mesh, and Alt. Fault 2 Mesh) and elastic dislocation modelling to calculate coseismic vertical surface displacements (Step 2 in Fig. 3; Fig. 4; See also Data Availability section). The earthquake rupture scenarios are defined from the SRM. Since the SRM includes nationwide ruptures (up to 1000 km), we only performed elastic dislocation modelling for earthquake rupture scenarios that include a fault subsection in our fault mesh sets. Earthquake scenarios that extended beyond the Wellington region were truncated at the mesh boundaries following sensitivity testing to establish which fault subsections could influence coastal VLM in the Greater Wellington Region (e.g., Fig. 4).

The slip distribution within individual earthquake rupture scenarios affects the resulting surface deformation. Therefore, we tested both uniform and tapered slip distributions for the crustal fault elastic dislocation models (Step 2 in Fig. 3). The slip taper follows a sine-square-root function, as used in the NZ NSHM 2022 (Thingbaijam et al., 2022). We used the fault subsection centroid to calculate the normalized distance, where the total distance follows the strike direction of the earthquake rupture scenario. Average slip is derived from the SRM branch solutions and varies based on fault source magnitude-frequency scaling relationships (Stirling et al., 2021). The uniform slip distribution applies the average slip value to all fault subsections.

For simplicity, we used uniform slip on the subduction interface meshes, as used in the NSHM. Onshore surface deformations are less sensitive to variations in slip at the depths of the subduction interface (c. 15-30 km) and the fault subsections from the SRM are much larger than for crustal faults. Down-dip slip is uniform for both crustal and subduction earthquake scenarios, as in the NZ NSHM 2022 (Gerstenberger et al., 2022b, 2024b).

Surface displacements were calculated using the method of Nikkhoo and Walter (2015) and a Poisson ratio of 0.25. We calculated displacements for all earthquake scenarios at 13 sites along the Wellington Region coastline for probability calculations. These sites cover a wide spatial distribution and coincide with population centers or critical infrastructure (Fig. 2C). As two sites in Porirua (Porirua CBD south, Porirua CBD north) have c. 1 km separation, only Porirua CBD north is shown in most results figures to reduce redundancy. The earthquake scenario displacement calculations were repeated for all branches in the SRM logic trees for all meshes. Additional grid-based elastic dislocation models illustrate individual earthquake scenario displacements but were not used in the probabilistic analyses.

3.4 100-Year Cumulative Displacements

The probability of an earthquake (and ultimately, the probability of coseismic displacement) relies on annual rates from the SRM solutions. The displacements used for probability calculations in this study represent cumulative displacement (i.e., from one or more earthquakes) within 100-year intervals. The cumulative coseismic vertical displacements can result from three different source types: crustal-fault only, subduction-interface only, or combined crustal-subduction models.

We define a ‘source model’ here as a specific combination of fault mesh(es), slip distribution (uniform or tapered), and associated logic tree branches and solutions. The earthquake catalogue, branch parameters, and solution rates for all crustal-fault-only and subduction-interface-only fault models are defined in the SRM (Gerstenberger et al., 2022a, 2022b, 2024b, 2024a). The combined crustal-subduction source branches consist of all unique pairings from the crustal-only and subduction-only logic-tree branches; it is effectively a combined catalogue of earthquake scenarios and annual rates. An inherent assumption in this process is that crustal fault and subduction interface earthquakes rupture independently. This study does not consider joint subduction-crustal ruptures or earthquake sequences.

For each branch in a source model, we simulated combinations of earthquake scenarios and displacements for many synthetic 100-year time intervals (Step 3, Fig. 3). For the crustal-only and subduction-only source model branches, we simulated n=1,000,000 intervals. For the pairs of crustal fault-subduction interface source model branches, we simulated *n*=100,000 intervals instead, for computational efficiency.

We modelled which earthquakes occurred in each simulated 100-year interval using the following approach. First, for each earthquake rupture with a non-zero annual probability in the SRM branch of interest, we sampled a Poisson distribution to model the number of times that earthquake rupture occurs during the simulated 100-year time window. As a rate parameter for the Poisson distribution, we used the SRM branch annual probability for the earthquake rupture of interest. For each SRM branch (both subduction and crustal), there are typically 100-300 ruptures with non-zero annual probabilities. Annual probabilities for each earthquake rupture are sufficiently low that in practice each rupture almost always occurs either once or not at all in a given 100-year time window.

Second, for the earthquakes that were modeled to have occurred during the 100-year time window of interest, we simulated the displacement at each site from that earthquake. A first order estimate of the displacement — "average displacement" hereafter — at each site was calculated using magnitude-area scaling and the approach in Section 3.2, but we also introduced noise in modelled displacements to account for site displacement uncertainty. This noise was introduced by sampling a random value from a normal distribution with μ=1 and σ=0.4, and multiplying that random value with the modelled "average displacement" at the site of interest. The main purpose of introducing the noise was to overcome the fact that we modelled very simple slip distributions and material properties to give the "average displacement" (Section 3.2). However, in reality, the earthquake slip distribution and crustal elastic properties will both be heterogeneous, affecting the displacement at each site. The value of σ=0.4 is somewhat arbitrary and could be refined in future work; we chose it to give a conservative estimate of displacement uncertainty at our sites — 68% of modelled displacements are between 0.6 and 1.2 x the "average displacement", while 95% of displacements are between 0.2 and 1.8 x the average.

Finally, displacements at each site were summed across all the earthquakes modelled to have occurred in the 100-year window of interest. Displacements from the *n* synthetic 100-year windows were combined to create hazard curves.

3.5 Probability Calculations and Modelling Products

A primary product of a PSHA is a hazard curve, which graphically shows the probabilities of exceeding different ground motion thresholds. Similarly, for the PCDHM in this study, we show the probability of exceeding different displacement thresholds in displacement hazard curves (step 4 in Fig. 3). However, the consequences associated with uplift and subsidence are not equal; therefore, uplift and subsidence displacement hazard curves are kept separate. Additionally, the net displacement (final displacement relative to zero initial displacement) may not equal the total displacement (amount of displacement, up or down, from all earthquakes) in 100-year intervals. Therefore, we calculate displacement exceedance probabilities and hazard curves for uplift, subsidence, and total-absolute-value vertical displacement for the 100-year time intervals.

The probabilities of exceedance are calculated based on the number of times coseismic displacement exceeded a threshold value in the *n* 100-year intervals. This was repeated for all uplift, subsidence, and total-absolute-value vertical displacement thresholds within a single source model branch.

Finally, we aggregated the probabilities from all source model branches into a weighted mean probability hazard curve. The branch weights for the crustal-fault only and subduction-interface only source models are from the SRM (step 5 in Fig. 3, flowchart) (Gerstenberger et al., 2022a, 2024a). The branch weights for the combined crustal and subduction source models are the product of the crustal fault and subduction interface branch weights. The errors depicted in the results figures indicate the maximum and minimum branch values in that fault model.

3.6 Limitations

In addition to the limitations caused by the using the SRM data and solutions (described above), there are several things this PCDHM does not do. First, we did not calculate lateral coseismic displacement; all displacements reported here are in the vertical direction. Next, we did not include the contributions from postseismic displacement. Postseismic displacement is typically orders of magnitude smaller than the coseismic displacement and will vary spatially based on the degree of after-slip and crustal properties (Luo and Wang, 2022). We also did not include interseismic displacement in these models. Some or all of these displacements may therefore be reversed following elastic behavior of a full seismic cycle, particularly for subduction interface ruptures (Savage, 1983).

Perhaps the most important caveat of this model is the resolution of both the input data and final products. The NZ NSHM 2022 and associated fault networks are at a national scale, therefore, the results in this PCDHM are also spatially coarse resolution. Additionally, the probabilities are averaged over many possible earthquakes on these simplified faults. In reality, km-scale fault trace complexity and the distribution of secondary ruptures, which can change from event to event even on a single fault, will influence site-specific vertical deformation in individual earthquakes (e.g., Clark et al., 2017; Morris et al., 2023; Scott et al., 2023).

This means that the results of this PCDHM should not be used for site specific hazard assessments, and resolution should always be considered when interpreting the results. In some instances, we discuss below how small changes in model inputs (e.g., fault geometry or site location) will impact the displacement hazard and probabilities. However, these effects are meant to convey broader scale processes, such as the impact of a chosen fault geometry on the model results. This model is designed to highlight how a national seismic hazard dataset may be used to estimate patterns coseismic displacement probabilities and inherently contains large uncertainties at a site-specific scale.

4. MODEL OUTPUT OVERVIEW AND EXAMPLES

This section provides an initial overview of the PCDHM results. Subsequent sections discuss the result sensitivity to fault geometry, slip distribution, and logic tree parameters as provided in the NZ NSHM 2022. In all instances, the highlighted results are intended to demonstrate the utility of the model and uncertainties therein.

The standard PCDHM outputs are hazard curves (e.g., Fig. 5). Displacement hazard curves graphically show the probabilities of exceeding all uplift, subsidence, or total movement thresholds at each site, but can be challenging to interpret. Therefore, we also show the displacements at specific probabilities of exceedance (10% and 2%) and the probabilities at specific displacement thresholds (0.2 m uplift/subsidence). The 0.2 m threshold is based on the average global mean sea-level rise (c. 0.17 m) over the 20th century and conservative estimated sea level rise (0.23 m) in A-NZ between 2020-2070; it is therefore likely to impact projected sea-level change hazards (Church et al., 2013; Ministry for the Environment, 2022). Below, we first describe example results from a single branch of a crustal-only source model (CFM Mesh geometry and uniform slip) and subduction interface-only fault model (with no dip modifications and uniform slip).

The subduction-only single-branch results are relatively simple because the interface is effectively one fault source with variations in slip location. At most sites, and for most displacement thresholds, the probabilities of coseismic subsidence are higher than the probabilities of uplift (Fig. 5). However, coseismic uplift probabilities are higher than subsidence probabilities at the eastern sites closest to the trench (Cape Palliser, Flat Point) (Fig. 5). At 10% probability of exceedance, the minimum coseismic displacement is near-zero (Fig. 6A). At 2% probability of exceedance, this subduction fault model branch yields larger minimum subsidence displacements for most sites except those along the east coast (Fig. 6A). These minimum displacements are not single-event displacements; instead, they reflect general trends of repeated earthquakes in the branch catalogue. Fig. 6B shows that the 0.2 m uplift exceedance probability is low (<5%) at most sites except those near the eastern coast (closest to the trench), with a maximum exceedance probability of 17%. The 0.2 m subsidence exceedance probabilities are lowest near Cape Palliser, reaching a peak of 16% at the sites around Wellington Harbour (Fig. 6B).

The crustal-only source model single branch results follow fewer consistent patterns between sites because they are influenced unequally by multiple crustal fault sources. For example, even between nearby sites like Petone and Wellington Central Business District (CBD) (~10 km distance), the relative relationships between uplift and subsidence exceedance probabilities vary (Fig. 7). The hazard results also vary by displacement threshold; for example, at the South Coast site, uplift is more likely at small displacement thresholds while subsidence is more likely at large displacement thresholds (Fig. 7). The 10% exceedance probability correlates to virtually no vertical deformation from the crustal-only fault model for all sites (Fig. 8A). At the 2% exceedance probability, relative uplift vs subsidence hazard varies significantly by site

(Fig. 8A). For example, Petone has larger minimum subsidence than uplift value (-0.8 vs +0.4 m), but Wellington Airport has a smaller minimum subsidence than uplift value (-0.1m vs +0.6 m) (Fig. 8A). The probabilities of exceeding 0.2 m subsidence or 0.2 m uplift range between 0-9% (Fig. 8B). The probability of subsidence is highest for this branch at sites from Petone to Cape Palliser, likely a reflection of the higher proportion of dip slip on faults between Wellington Harbour and offshore of the east coast.

The weighted mean hazard curves are the mean of all single-branch hazard curves in a fault model, weighted following the SRM logic tree (Gerstenberger et al., 2022a, 2024a). Fig. 9 shows an example of weighed mean results compared to all the branches for a crustal-only fault model. The full range of individual branch hazard curve results are used as error bars in subsequent plots (e.g., Figs. 9B, C). Many of the branch parameters have a sizable effect on displacement probabilities, therefore, the uncertainties for the weighted mean of the fault model are very wide (Fig. 9).

5. RESULTS

We tested PCDHM result sensitivity to various fault geometries, slip behaviour, and SRM logic tree parameters. For brevity in the following section, we focus on the subsidence probabilities unless otherwise noted. The slip distribution sensitivity tests use weighted mean probability results from a single crustal source model. All source model geometry sensitivity results show weighted mean results and uniform slip distribution. For the SRM logic tree parameter sensitivity tests, we focused on weighted mean results from uniform slip on one crustal source model.

5.1 Source model sensitivity testing

5.1.1 Influence of Subduction Interface Geometry

We tested whether increasing or decreasing the Hikurangi interface dip angle (and thus increasing or decreasing depth below the surface at each site) would change the probabilistic displacement results.

Subduction interface dip variations have a minor effect on the surface deformation from individual earthquakes but do not significantly change the weighted mean probabilistic displacement hazard outputs (Fig. 10). For individual earthquakes, a steeper interface dip reduces the coseismic uplift farther from the trench (i.e., near Wellington Harbour and the northwestern coast) but increases uplift slightly near the southeastern coast (e.g., Flat Point and Cape Pallier) (Fig. S2). The converse is true for uplift on the gentler-dip interface (Figs. S2). Changes in subsidence are smaller than changes to uplift, but do not follow as consistent a pattern. Coseismic subsidence from subduction interface earthquakes is controlled by down-dip extent of slip in each earthquake (e.g., Delano et al., 2023); therefore, by increasing the dip (and distance to the slip patch), the surface displacements are slightly reduced. Since the aggregate effects are relatively minor, for the remainder of this manuscript we only consider the unmodified subduction interface source model.

The subduction interface fault subsection shapes also influence the vertical displacement patterns and highlight how the coarse resolution of this model can impact site-specific results. The interface mesh fault subsections are derived from the rectangular NZ NSHM 2022 patches, creating jagged rupture edges (Fig. 4B). Consequently, the jagged edge of the earthquake scenario slip patches is reflected in the surface deformation for individual earthquakes (Fig. 4B). We applied discretization by fault subsection depth (rather than geographic location) which smoothed some jagged rupture edges but did not eliminate them (S3-S4). The probability results are averaged over many events, so the effects are greatest at eastern sites where the interface is shallower and at higher displacement thresholds (Fig. S5). These artifacts cannot be entirely removed without drastically changing the fault subsection shape (as used in the NZ NSHM 2022), but future work could potentially use other smoothing to reduce them.

5.1.2 Influence of crustal fault source geometry

The three different crustal source mesh geometries have several significant effects on coseismic displacement hazard, but the impacts to the results vary by site and proximity to specific faults (Fig. 11). For example, we examined the influence of small dip and rake differences on faults near Porirua (Fig. 12, Table S1). In individual earthquakes, the slight dip-slip component in the Alt. Fault 1 and 2 Meshes (Fig. 12A) generates uplift and subsidence adjacent to the fault compared to effectively no vertical deformation from the CFM Mesh. The weighted mean uplift and subsidence exceedance probabilities are therefore much larger at South Coast, Porirua, and Paraparaumu in the alternative geometry fault meshes compared to the CFM Mesh (Figs. 11-12). The slight dip-slip component also creates a larger hazard difference across the fault; a vertical pure strike-slip fault produces nearly symmetrical hazard on either side of the fault, but dipping faults affect both sides unequally (Fig. 12). The modelled effects at Porirua are illustrative only; the modelled Ohariu and adjacent faults are highly simplified compared to the mapped fault traces in the active fault database (Langridge et al., 2016).

The gentler reverse fault dips in Alt. Fault 2 Mesh compared to the CFM Mesh (Fig. 2C) result in broader hanging wall uplift per earthquake. This generates overall greater uplift exceedance probabilities the Cape Palliser and Lake Ferry sites. Gentler fault dips also increase the coseismic subsidence magnitude and shift hanging wall subsidence farther from the fault trace, resulting in higher subsidence hazard west of Lake Ferry (Fig. 11).

The longer Palliser-Kaiwhata fault in both alternative crustal meshes greatly increases the uplift and decreases the subsidence probabilities at Cape Palliser and Lake Ferry (Fig. 11, S6). In the CFM Mesh results, the majority of slip and surface deformation from the Palliser-Kaiwhata Fault is north of Cape Palliser (e.g., Flat Point), and the dominant crustal fault deformation is hanging wall subsidence from other offshore reverse structures. Subsidence west of Cape Palliser is also affected by a longer Palliser-Kaiwhata Fault; it is the only fault geometry change east of Wellington Harbour in the Alt. Fault 1 Mesh, and therefore appears to have influenced the subsidence probabilities at Turakirae Head by shifting the earthquake scenario slip patches below the site (Figs. 2C, 11).

In the Alt. Fault 2 Mesh, the Wellington-Hutt Valley Fault dips northwest (compared to southeast in the CFM and Alt. Fault 1 Meshes; Figs. 2) though the relative displacement sense (down-to-the-southeast) remains the same as the other meshes. This single change does not appear to have a great effect on hazard probabilities at nearby sites (e.g., Petone and Seaview) depicted by similar displacements between the Alt. Fault 1 and 2 meshes (Fig. 11B). However, sites near Wellington Harbour are impacted by many crustal fault sources that vary in geometry between meshes. It is difficult to separate the effects of the Wellington-Hutt Valley Fault from the others.

These results highlight that even small changes in dip, rake, or fault length may impact the vertical deformation probabilities significantly. These probabilities, however, represent the cumulative effect from many crustal faults; small uncertainties on several structures can have much larger or smaller effects when considered together. This suggests that individual site analyses may be needed to incorporate more detailed fault data, consider if faults may change dip at depth, or investigate whether small variations in slip behavior will affect the displacement hazard. The remainder of the sensitivity analyses described below only focus on the CFM Mesh, but the results vary greatly between different crustal fault meshes.

5.1.3 Impact of crustal fault slip distribution

The crustal fault slip distribution (uniform vs tapered) changes the displacement pattern for individual earthquake rupture scenarios (Fig. S7) but in aggregate does not significantly change the overall displacement hazard (Fig. 13). The Monte Carlo simulations over 10^5-10^6 100-year intervals, as well as the displacement uncertainties (i.e., ±40%) effectively smooth the displacement variations caused by individual fault ruptures. In these tests, the uniform slip distribution has slightly higher probabilities of exceedance at most of our test sites. Therefore, we show uniform slip distribution source models for all subsequent results.

The difference between slip taper effects on single-earthquake displacements compared to probabilistic displacement hazard highlights the importance of scale. Displacement probabilities are inherently smoothed over many earthquakes and 100-year intervals; however, actual hazard experienced in the next 100 years is the result of one (or a few) earthquakes. The slip distribution from individual earthquake ruptures is therefore still important for site-specific analyses but is not investigated further here.

5.2 Logic Tree Parameter Sensitivity Testing

The following sensitivity tests apply to logic tree branch parameters as defined by the fault source type (crustal faults or Hikurangi interface) in the SRM. For clarity of explanation the results below detail the effects for one source model—the crustal-only CFM Mesh and uniform slip—unless otherwise noted. We show results for three sites across the Wellington region.

5.2.1 Time-Dependence Logic-Tree Parameter

The time-dependence parameter is only in the crustal fault source logic tree (Gerstenberger et al., 2022a, 2024a). This is a conditional parameter based on earthquake recurrence intervals and the time since rupture for faults that have hosted recent earthquakes or have fast slip rates (Gerstenberger et al., 2022b, 2024b). To simplify, the time-dependent branches have a higher rupture rate on faults with high slip rates that have not experienced a recent earthquake (Gerstenberger et al., 2022b, 2024b).

The time-dependence parameter does not significantly change the subsidence exceedance probabilities across the crustal fault model branches (Fig. 14A). There are some sites where time-dependent branches have higher probabilities than time-independent branches, and vice-versa, but the patterns likely depend on the proximity to faults determined to be late in their seismic cycles.

5.2.2 Deformation Model Logic-Tree Parameter

The SRM deformation model parameter (i.e., geologic or geodetic) controls the locations and slip rates imposed on crustal fault subsections (Gerstenberger et al., 2022b, 2024b). The different slip rates are derived from either the longer-term geologic record (10^3 –10^5 yrs) or more short-term geodetic data (10^1 yrs). This ultimately affects the NZ NSHM 2022 annual rate solutions for earthquake rupture scenarios in each branch.

The deformation model parameter significantly impacts the crustal fault coseismic displacement hazard (Fig. 14B). The differences between the geologic and geodetic deformation models are fault-specific and thus, for the displacement probabilities here, are site-specific and threshold-specific. Overall, the geologic deformation model branches generally have higher subsidence probabilities than geodetic deformation model, but the difference is less pronounced for the eastern sites (Fig. 14B). This is because certain faults, or certain fault subsections, have faster slip rates and higher earthquake recurrence in the geologic deformation model than the geodetic deformation model (Gerstenberger et al., 2022b, 2024b).

Additional information about fault behavior may help determine whether the geologic or geodetic model is more appropriate, but on a fault-specific basis. Alternatively, incorporating the higher displacement probabilities (regardless of deformation model type) may be a more conservative approach for future displacement hazard studies.

5.2.3 Non-Stationary Moment-Rate Scaling Parameter Sensitivity

The non-stationary moment-rate scaling parameter (S-value) scales the annual rate of earthquake occurrence for each earthquake rupture scenario for both the crustal and subduction sources (Gerstenberger et al., 2022b, 2024b). The crustal fault rates are scaled by 0.66, 1.00, and 1.41; the subduction interface rates are scaled by 0.42, 1.00, and 1.58 (Gerstenberger et al., 2022b, 2024b). For this PCDHM, the S-value ultimately modulates the frequency of earthquakes in the 100-year intervals at the Monte-Carlo simulation (Step 3 in Fig. 3).

The coseismic displacement hazard results are similarly and predictably influenced; branches with smaller scaling factors (i.e., lower earthquake rates) have lower probabilities of exceedance and branches with larger scaling factors (i.e., higher earthquake rates) have higher probabilities of exceedance (Fig. 14C).

5.2.4 Magnitude-Frequency Distribution Parameter Sensitivity

The magnitude frequency distribution parameters (paired b- and N-values) control the overall distribution of earthquake magnitudes and the number of earthquakes > Mw 5.0 (Gerstenberger et al., 2022b, 2024b). Smaller b- and N-values yield a lower frequency of small-magnitude earthquakes for the same moment release (Gutenberg and Richter, 1944).

These parameters have a sizable impact on the displacement probability results for the crustal-only source model shown; smaller b- and N-values result in higher displacement probabilities than larger ones (Fig. 14D). This general trend is also true for the subduction interface-only source model, but the results vary more across the displacement thresholds (Figs. S8-S9).

These results suggests that infrequent, larger-magnitude earthquakes are to some extent controlling the displacement hazard over the 100-year intervals, but this parameter might warrant additional investigation or refinement in future work.

5.3 Relative Contributions from Subduction Interface and Crustal Faults

The relative contributions from the crustal fault and subduction interface sources on coseismic displacement vary depending on the type of displacement (uplift, subsidence, or absolute value displacement), the crustal fault mesh used, and the site location. We focus here on the weighted mean subsidence results for crustal-only, subduction-only, and combined crustal-subduction source models using the Alt. Fault 2 Mesh, unmodified subduction interface mesh, and uniform slip (Fig. 15). The Alt. Fault 2 mesh is shown for crustal faults because the overall gentler fault dips result in a more conservative hazard estimate. As demonstrated in the sections above, however, the localized displacement exceedance probabilities can vary widely depending on displacement direction (uplift or subsidence), fault geometry, and logic tree parameters.

In general, the subduction interface-only source model produces higher subsidence hazard than crustal fault sources near the west and east coasts, and nearly the same subsidence hazard as crustal faults near Wellington Harbour (Fig. 15). Subduction interface subsidence hazard generally increases away from the trench (i.e., to the northwest), although is locally high at Flat Point. For the 0.2 m minimum subsidence threshold, these probabilities generally vary between 0-20% (weighted mean) for the subduction interface.

The probability of subsidence from the crustal-only source model is more spatially variable (i.e., between sites) based on the proximity to specific faults (Fig. 15). The highest probabilities for the 0.2 m subsidence threshold are located in the northeastern Wellington Harbour (i.e., in the hanging wall of the normal-oblique Wellington-Hutt Valley fault) (Fig. 15). The crustal-only subsidence probabilities of exceedance range from 0-16% (weighted mean).

At most sites, both crustal and subduction faults independently produce earthquakes with subsidence. At a few sites, the combined crustal-subduction source has a lower subsidence hazard than the subduction-only models (e.g., Cape Palliser and Paraparaumu, Fig. 15B, C). Additionally, at most sites, the combined source subsidence hazard is smaller than the sum of the crustal-only and subduction-only model probabilities (Fig. 15C). These results both occur because uplift and subsidence (from different earthquakes) may both occur in the same 100-year time interval; the uplift signal effectively 'cancels' some of the subsidence for that time-interval.

5.4 Combined Fault Source Displacement Hazard Results

The combined source (crustal and subduction) is most pragmatic for planning purposes because the crustal and subduction sources both contribute to hazard. Figure 16 shows combined hazard results from the crustal Alt. Fault 2 and subduction interface sources, shown in spatial and tectonic context. The results do not include earthquake triggering from one source fault to another, or probabilities for specific joint subduction-crustal ruptures.

Most sites have a significant probably of both coseismic subsidence and uplift over a 100-yr interval (Fig. 16). Towards the eastern coast, the minimum uplift is greater than the minimum displacement at the 2% probability threshold (Fig. 16A). Elsewhere, the minimum displacements are of similar magnitude, or slightly larger for subsidence at the 2% probability threshold. Near Wellington Harbour, the coseismic subsidence hazard exceeds the uplift hazard because multiple fault sources are contributing to coseismic subsidence more often, and in larger amounts, than fault sources that produce coseismic uplift. Note that these coseismic displacement hazard results are not indicative of long-term geologic displacement (See section 6.1 below).

Figure 16B shows the combined source probabilities for exceeding 0.2 m subsidence, which range from 6–29% (weighted mean values). The highest probabilities are near Wellington Harbour, which occupies the down-thrown side of the fast-slipping Wellington-Hutt Valley Fault as well as subsidence hazard from the subduction interface.

6. DIRECTIONS OF FUTURE WORK

6.1 Comparison with the Geomorphic Record

A logical test of a probabilistic model is to compare site results to the longer-term geomorphic and geologic record as a means of validation. However, these PCDHM results cannot be directly compared to the geomorphic record for a few reasons.

First, the modelled coseismic displacements represent a mix of permanent and elastic tectonic deformation while the geomorphic record shows net permanent deformation over several earthquake cycles. The minimum displacements and uplift/subsidence probability results shown here are not indicative of long-term deformation. For example, subduction earthquake displacement is primarily elastic and only a small portion (< 10%) persists over many earthquake cycles (e.g., Briggs et al., 2008; Wesson et al., 2015; Jolivet et al., 2020). In contrast, dip-slip crustal faults can cause permanent uplift or subsidence by thickening or thinning the upper plate along the fault surface (Begg and Mazengarb, 1996; Begg and McSaveney, 2005; Paquet et al., 2011; Berryman et al., 2018; Ninis et al., 2023) but distal displacement can be elastically recovered (e.g., Delano et al., 2023). Therefore, the coseismic displacements modelled here would mostly over-estimate contributions to the geomorphic record, but the degree would vary by site and fault source contributions. As an example, the Seaview site may experience near-equal coseismic uplift and subsidence hazard (e.g., Fig. 16), but much of the coseismic subsidence is likely to be recovered (reversed) over a full seismic cycle.

Next, the simplified fault network yields much coarser displacement patterns than the geomorphic record. Kilometer-scale variation in fault geometry and complex fault connectivity clearly influences coseismic displacement behavior (Clark et al., 2017; Litchfield et al., 2018), but is too computationally intensive or uncertain to model here. For example, a flight of Holocene beach ridges and marine terraces at Turakirae Head demonstrate repeated coseismic uplift, with the most recent uplift of up to 6.4 m from the 1855 Wairarapa earthquake (McSaveney et al., 2006). In our crustal-only fault models shown here, Turakirae Head experiences near equal coseismic uplift and subsidence from the adjacent modelled Wharekauhau Thrust and Wairarapa Faults (Fig. 16A). This model does not capture complex fine-scale fault interactions, trace locations, slip partitioning and distribution, and subsurface fault geometry.

Finally, slip rates in the SRM are partially based on geologic and geomorphic displacement rates (Gerstenberger et al., 2022b, 2024b) and contribute to the earthquake slip and frequency in this model. Thus, comparing these model results to the geomorphic record is not a true validation, because some of the data are circular.

6.2 Considerations for Additional Modelling

Many parameters in this PCDHM are directly tied to the NZ NSHM 2022, which is tuned for ground motion hazards rather than coseismic displacement hazards. In some instances, branches of the NZ NSHM 2022 logic tree were omitted from the final model because they did not impact the seismic hazard results (e.g., magnitude-scaling relationship C-value) (Gerstenberger et al., 2022a, 2024a). It is possible that some of these branches would affect results for this PCDHM, but we did not perform sensitivity tests on those parameters. A future iteration of this model may require a bespoke weighting that is sympathetic to fault displacement hazards instead of ground motions.

We highlighted above that fault geometry can significantly affect displacements and the associated exceedance probabilities. Even with the alternative crustal fault models, the fault geometries here are still simplified and generally omit significant changes in dip or strike. Moving toward a more realistic fault mesh may yield more realistic results, but without detailed understanding of fault geometry at depth, the uncertainties from geometry will remain wide. For listric faults, adopting a low average dip may also yield more realistic results than the steeper dips presented in the CFM. For the subduction interface, it may be more appropriate to use smaller fault subsections to reduce the surface effects of rectangular patches. Adjusting crustal fault geometries, however, is best done in tandem with the NZ NSHM 2022 in order to share the source fault data, earthquake rupture scenarios, logic tree parameters, and branch weights.

For the subduction interface models in particular, and potentially for the crustal source models, the inclusion of spatially heterogeneous elastic properties may influence the modelled surface deformation in individual earthquake scenarios (Williams and Wallace, 2018). We did not include spatial heterogeneity to reduce the computation intensity; however, it is unlikely to influence the results more than the logic tree parameters or when considered in aggregate over all events in a branch. Future investigations may want to consider elastic heterogeneity in concert with subduction interface slip distribution modifications.

Additional uncertainties exist that are challenging to include here and in the NZ NSHM 2022. Fault rupture behavior uncertainties stem from a limited understanding of fault rupture connectivity as well as how stress transfers between the interface and overlying crustal faults. Further, the sheer number of active and inherited structures in Aotearoa New Zealand are not all represented by the CFM. There are several near-surface effects that cannot be captured at the scale of this model that stem from fault complexity, local geologic conditions, and distributed or partitioned deformation. Inelastic and site-specific conditions can contribute to anomalously large surface deformations, as was observed near the Kekerengu fault from the 2016 Kaikōura earthquake (Clark et al., 2017). These effects would be impractical to model but could potentially be incorporated in hazard assessments based on local geologic conditions (e.g. near alluvial deposits). Many additional factors complicate earthquake behavior but are difficult to constrain and may be spatially or temporally variable, such as the influence of subduction zone fluids, degree of plate coupling, and heterogeneous crustal properties.

7. POTENTIAL IMPLICATIONS

We focused here on the coastlines of the Wellington Region because it occupies a complex tectonic setting that experiences coseismic displacement from both the Hikurangi subduction interface and multiple crustal fault sources. Additionally, the 1855 Wairarapa earthquake demonstrated how earthquakes in the Wellington Region can drastically alter the coast and impact infrastructure and development (Grapes and Downes, 1997). The main aim of this study was to use the existing seismic hazard models and datasets from the NZ NSHM 2022 to assist in answering questions like, “what is the probability of coseismic vertical displacement along the coastline over 100 years?”

This first iteration of a coastal-focused PCDHM successfully repurposed the NZ NSHM 2022 data to create displacement hazard products. The limitations are primarily due to the spatial and temporal scale of the datasets and uncertainty in earthquake behavior and crustal fault geometries. Additionally, the CFM and other NZ NSHM 2022 components were developed and sensitivity tested for seismic hazard assessments rather than coseismic displacement hazard models. This PCDHM is therefore not well suited to fine-scale analyses without additional site-specific conditions and more detailed fault data, but instead provides a regional overview.

Despite these limitations, several key findings have emerged for the Wellington Region. First, most sites have some likelihood of experiencing substantial (0.2 – 2.0 m) coseismic uplift and subsidence over a 100-year period (Fig. 16). Importantly, this magnitude of coseismic displacement can originate from both subduction interface and crustal fault sources. The subduction interface contributes more to the subsidence hazard at most sites than CFM crustal fault sources, but this gap is narrower when alternative crustal fault mesh geometries are considered. At most sites, neither fault source type dominates all vertical displacement probabilities.

Evaluating the probabilities of displacements from all fault sources is important because the limited historical and geomorphic record does not reflect the range in possible coseismic displacement behaviors. The only historical coast-deforming earthquake in the Wellington Region (1855 Wairarapa earthquake) caused widespread uplift, transformed the landscape, and aided regional development and expansion. Most of the geomorphic record preserves permanent crustal-fault uplift, but this is likely influenced by preservation potential, earthquake cycle elastic recovery, and the interactions between successive coseismic displacements (e.g., Grapes and

Downes, 1997; McSaveney et al., 2006; Ninis et al., 2023). However, the next earthquake may produce subsidence along at least parts of the coastline.

We approached probabilistic displacement hazard from a multi-hazard perspective that considers all coseismic vertical displacement, rather than focusing on differential offset across surface fault ruptures. Even small amounts of coseismic subsidence can exacerbate the effects of other hazards such as surface and groundwater flooding, tsunami inundation, and storm surge waves (Fig. M1). Coseismic subsidence will compound the effects of ongoing global sea-level rise (Fig. M1). These hazards are not limited to the Wellington Region, and similar probabilistic models will be useful elsewhere in Aotearoa New Zealand and globally where a dense fault network interacts with the coast (e.g., Hawke's Bay and Bay of Plenty, New Zealand and other subduction margins).

8. CONCLUSIONS

This study provides a framework for the first probabilistic coseismic displacement hazard model at a regional scale using a national earthquake hazard model as a basis. In settings with multiple active fault sources, the direction of coseismic displacement is variable from one earthquake to the next. The spatial patterns, displacement direction, and magnitudes of displacement are sensitive to factors such as fault source location and geometry as well as slip location and direction. A probabilistic approach is useful to capture the range in these variables for long-term planning and engineering purposes.

Coseismic vertical displacement can instantaneously cause relative sea level changes equivalent to the effect of decades or centuries of changes from other factors. Coseismic subsidence can compound hazards like tsunami and coastal flooding but is more spatially variable and stochastic than climate-driven global mean seal level rise.

This model provides a highly customizable framework that can be expanded to additional locations, updated to incorporate new data, or modified based on planning objectives. The results from this PCDHM are a useful complement to geological investigations that use geomorphic and sedimentary records to understand past earthquakes. Geologic investigations, historical observations, and site-specific investigations provide the short and long-term data about earthquake and fault behavior that are necessary to constrain earthquake hazard models. This PCDHM aggregates data and uncertainties from multiple complex sources for regional-scale comparisons and decision-making.

We highlight several limitations of this regional-scale model and approach, but the framework developed here is applicable to other settings globally. In particular, this approach is most useful where multiple fault sources contribute to coseismic vertical deformation and in settings sensitive to small amounts of regional displacement (e.g., coastal settings).

SUPPLEMENTARY FILES AND DATA REPOSITORY

[1]Supplemental Material. The supplementary files include Figures S1–S8 and Table S1 that provide additional modeling data and results. Please visit https://doi.org/10.1130/XXXX to access the supplemental material, and contact editing@geosociety.org with any questions. All scripts used in this manuscript are available on the Zenodo/GitHub repository (Delano et al., 2024)

ACKNOWLEDGMENTS

This manuscript was funded by the University of Canterbury Mason Trust, It's Our Fault Programme (funded by Toka Tū Ake Natural Hazards Commission, Wellington City Council and the Wellington Regional Emergency Management Organisation), and QuakeCoRE. It was also funded by a New Zealand Ministry of Business, Innovation, and Employment Grant through Victoria University of Wellington (RTVU2206), Our changing coast – Sea-level rise on Aotearoa's dynamic margin Programme, the National Seismic Hazard Model Programme (contract 2020-BD101), and the National Science Challenges via the Resilience to Nature's Challenges Earthquake and Tsunami Programme (contract C05X1901). This paper was improved by discussions with Chris DiCaprio, Russ Van Dissen, and Stuart Henrys.

REFERENCES CITED

Amos, C.B., Burbank, D.W., Nobes, D.C., and Read, S.A.L., 2007, Geomorphic constraints on listric thrust faulting: Implications for active deformation in the Mackenzie Basin, South Island, New Zealand: Journal of Geophysical Research: Solid Earth, v. 112, p. B03S11, doi:10.1029/2006JB004291.

Barnes, P.M., Nicol, A., and Harrison, T., 2002, Late Cenozoic evolution and earthquake potential of an active listric thrust complex above the Hikurangi subduction zone, New Zealand: GSA Bulletin, v. 114, p. 1379–1405, doi:10.1130/0016-7606(2002)114<1379:LCEAEP>2.0.CO;2.

Beanland, S., and Haines, J., 1998, The kinematics of active deformation in the North Island, New Zealand, determined from geological strain rates: New Zealand Journal of Geology and Geophysics, v. 41, p. 311–323, doi:10.1080/00288306.1998.9514813.

Beavan, J., and Darby, D., 2005, Fault slip in the 1855 Wairarapa earthquake based on new and reassessed vertical motion observations: did slip occur on the subduction interface?, *in* Proceedings Volume, Wellington, New Zealand, Greater Wellington Regional Council, p. 31–41, https://docs.niwa.co.nz/library/public/0909016879.pdf#page=41.

Beavan, J., Tregoning, P., Bevis, M., Kato, T., and Meertens, C., 2002, Motion and rigidity of the Pacific Plate and implications for plate boundary deformation: Journal of Geophysical Research: Solid Earth, v. 107, p. ETG 19-1-ETG 19-15, doi:10.1029/2001JB000282.

Bray, J.D., Seed, R.B., Cluff, L.S., and Seed, H.B., 1994, Earthquake Fault Rupture Propagation through Soil: Journal of Geotechnical Engineering, v. 120, p. 543–561, doi:10.1061/(ASCE)0733-9410(1994)120:3(543).

Budnitz, R.J., Apostolakis, G., and Boore, D.M., 1997, Recommendations for probabilistic seismic hazard analysis: Guidance on uncertainty and use of experts: NUREG/CR--6372-Vol.1, UCRL-ID--122160, 479072, NUREG/CR--6372-Vol.1, UCRL-ID--122160, 479072 p., doi:10.2172/479072.

Church, J.A., Clark, P.U., Cazenave, A., Gregory, J.M., Jevrejeva, S., Levermann, A., Merrifield, M.A., Milne, G.A., Nerem, R.S., and Nunn, P.D., 2013, Sea level change. In: Climate Change 2013: The Physical Science Basis. Contribution of Working Group I to the Fifth Assessment Report of the Intergovernmental Panel on Climate Change (T. F. Stocker, Qin, D., G.-K. Plattner, M. M. Tignor, S. K. Allen, J. Boschung, A. Nauels, Y. Xia, V. Bex, & P. M. Midgley, Eds.): Cambridge, United Kingdom and New York, NW, USA, Cambridge University Press.

Clark, K.J. et al., 2017, Highly variable coastal deformation in the 2016 MW7.8 Kaikōura earthquake reflects rupture complexity along a transpressional plate boundary: Earth and Planetary Science Letters, v. 474, p. 334–344, doi:10.1016/j.epsl.2017.06.048.

Cornell, C.A., 1968, Engineering seismic risk analysis: Bulletin of the Seismological Society of America, v. 58, p. 1583–1606, doi:10.1785/BSSA0580051583.

Darby, D.J., and Beanland, S., 1992, Possible source models for the 1855 Wairarapa Earthquake, New Zealand: Journal of Geophysical Research, v. 97, p. 12375, doi:10.1029/92JB00567.

Delano, J.E., Howell, A., Clark, K.J., and Stahl, T.A., 2023, Upper plate faults may contribute to the paleoseismic subsidence record along the central Hikurangi subduction zone, Aotearoa New Zealand: Geochemistry, Geophysics, Geosystems, v. 24, p. e2023GC011060, doi:10.1029/2023GC011060.

Delano, J., Howell, A., and McGrath, J., 2024, jedelano/Probabilistic_Coseismic_Displacement_Hazard_Model: for_submission:, doi:10.5281/ZENODO.13263930.

Field, E.H. et al., 2017, A Synoptic View of the Third Uniform California Earthquake Rupture Forecast (UCERF3): Seismological Research Letters, v. 88, p. 1259–1267, doi:10.1785/0220170045.

Gerstenberger, M.C. et al., 2024a, The 2022 Aotearoa New Zealand National Seismic Hazard Model: Process, Overview, and Results: Bulletin of the Seismological Society of America, v. 114, p. 7–36, doi:10.1785/0120230182.

Gerstenberger, M.C. et al., 2024b, The Seismicity Rate Model for the 2022 Aotearoa New Zealand National Seismic Hazard Model: Bulletin of the Seismological Society of America, v. 114, p. 182–216, doi:10.1785/0120230165.

Gerstenberger, M.C., Bora, S.S., Bradley, B.A., DiCaprio, C., Van Dissen, R.J., Atkinson, G.M., Chamberlain, C., Christophersen, A., Clark, K.J., and Coffey, G.L., 2022a, New Zealand National Seismic Hazard Model 2022 revision : model, hazard and process overview:, doi:10.21420/TB83-7X19.

Gerstenberger, M.C., Van Dissen, R.J., Rollins, C., DiCaprio, C., Chamberlain, C., Christophersen, A., Coffey, G.L., Ellis, S.M., Iturrieta, P., and Johnson, K.M., 2022b, The Seismicity Rate Model for the 2022 New Zealand National Seismic Hazard Model:, doi:10.21420/2EXG-NP48.

Grapes, R., and Downes, G., 1997, The 1855 Wairarapa, New Zealand, earthquake- analysis of historical data: Bulletin of the New Zealand Society for Earthquake Engineering, v. 30, p. 271–368, doi:10.5459/bnzsee.30.4.271-368.

Gutenberg, B., and Richter, C.F., 1944, Frequency of earthquakes in California: Bulletin of the Seismological society of America, v. 34, p. 185–188.

Hamling, I.J., Wright, T.J., Hreinsdóttir, S., and Wallace, L.M., 2022, A snapshot of New Zealand’s dynamic deformation field from Envisat InSAR and GNSS observations between 2003 and 2011: Geophysical Research Letters, v. 49, doi:10.1029/2021GL096465.

Heintz, J.A., Hortacsu, A., and McKenney, C., 2022, Earthquake-resistant design concepts: An introduction to seismic provisions for new buildings, Second Edition: FEMA P-749, https://www.wbdg.org/FFC/DHS/fema_p749_2022.pdf.

Henrys, S. et al., 2013, SAHKE geophysical transect reveals crustal and subduction zone structure at the southern Hikurangi margin, New Zealand: Sahke Geophysical Transect: Geochemistry, Geophysics, Geosystems, v. 14, p. 2063–2083, doi:10.1002/ggge.20136.

International Atomic Energy Agency, 2021, An Introduction to Probabilistic Fault Displacement Hazard Analysis in Site Evaluation for Existing Nuclear Installations: Vienna, INTERNATIONAL ATOMIC ENERGY AGENCY, TECDOC Series 1987, https://www.iaea.org/publications/14915/an-introduction-to-probabilistic-fault-displacement-hazard-analysis-in-site-evaluation-for-existing-nuclear-installations.

King, D.J., Newnham, R.M., Rees, A.B.H., Clark, K.J., Garrett, E., Gehrels, W.R., Naish, T.R., and Levy, R.H., 2024, A ~200-year relative sea-level reconstruction from the Wellington region (New Zealand) reveals insights into vertical land movement trends: Marine Geology, v. 467, p. 107199, doi:10.1016/j.margeo.2023.107199.

Lamarche, G., Proust, J.-N., and Nodder, S.D., 2005, Long-term slip rates and fault interactions under low contractional strain, Wanganui Basin, New Zealand: Tectonics, v. 24, p. n/a-n/a, doi:10.1029/2004TC001699.

Langridge, R.M. et al., 2016, The New Zealand active faults database: New Zealand Journal of Geology and Geophysics, v. 59, p. 86–96, doi:10.1080/00288306.2015.1112818.

Litchfield, N.J. et al., 2014, A model of active faulting in New Zealand: New Zealand Journal of Geology and Geophysics, v. 57, p. 32–56, doi:10.1080/00288306.2013.854256.

Little, T.A., and Rodgers, D.W., 2005, Co-seismic slip during the 1855 earthquake, southern Wairarapa Fault, New Zealand, *in* Proceedings Volume, Wellington, New Zealand, Greater Wellington Regional Council, p. 11–20, https://docs.niwa.co.nz/library/public/0909016879.pdf#page=41.

Little, T.A., Van Dissen, R., Schermer, E., and Carne, R., 2009, Late Holocene surface ruptures on the southern Wairarapa fault, New Zealand: Link between earthquakes and the uplifting of beach ridges on a rocky coast: Lithosphere, v. 1, p. 4–28, doi:10.1130/L7.1.

Luo, H., and Wang, K., 2022, Finding simplicity in the complexity of postseismic coastal uplift and subsidence following great subduction earthquakes: Journal of Geophysical Research: Solid Earth, v. 127, p. e2022JB024471, doi:10.1029/2022JB024471.

Ministry for the Environment, 2024, Coastal hazards and climate change guidance: Ministry for the Environment ME 1805, https://environment.govt.nz/assets/publications/Coastal-hazards-and-climate-change-guidance-2024-ME-1805.pdf.

Ministry for the Environment, 2022, Interim guidance on the use of new sea-level rise projections.: Ministry for the Environment ME 1667, https://environment.govt.nz/assets/publications/Files/Interim-guidance-on-the-use-of-new-sea-level-rise-projections-August-2022.pdf.

Morris, P., Little, T., Van Dissen, R., Hill, M., Hemphill-Haley, M., Kearse, J., and Norton, K., 2023, Evaluating 9 m of near-surface transpressional displacement during the M_w 7.8 2016 Kaikōura earthquake: re-excavation of a pre-earthquake paleoseismic trench, Kekerengu Fault, New Zealand: New Zealand Journal of Geology and Geophysics, v. 66, p. 244–262, doi:10.1080/00288306.2021.1954958.

Nicol, A., and Beavan, J., 2003, Shortening of an overriding plate and its implications for slip on a subduction thrust, central Hikurangi Margin, New Zealand: Tectonics, v. 22, p. n/a-n/a, doi:10.1029/2003TC001521.

Nicol, A., and Wallace, L.M., 2007, Temporal stability of deformation rates: Comparison of geological and geodetic observations, Hikurangi subduction margin, New Zealand: Earth and Planetary Science Letters, v. 258, p. 397–413, doi:10.1016/j.epsl.2007.03.039.

Nikkhoo, M., and Walter, T.R., 2015, Triangular dislocation: an analytical, artefact-free solution: Geophysical Journal International, v. 201, p. 1119–1141, doi:10.1093/gji/ggv035.

Ninis, D., Howell, A., Little, T., and Litchfield, N., 2023, Causes of permanent vertical deformation at subduction margins: Evidence from late Pleistocene marine terraces of the southern Hikurangi margin, Aotearoa New Zealand: Frontiers in Earth Science, v. 11, p. 1028445, doi:10.3389/feart.2023.1028445.

Okada, Y., 1985, Surface deformation due to shear and tensile faults in a half-space: Bulletin of the Seismological Society of America, v. 75, p. 1135–1154, doi:10.1785/BSSA0750041135.

Savage, J.C., 1983, A dislocation model of strain accumulation and release at a subduction zone: Journal of Geophysical Research: Solid Earth, v. 88, p. 4984–4996, doi:10.1029/JB088iB06p04984.

Scott, C. et al., 2023, Evaluating how well active fault mapping predicts earthquake surface-rupture locations: Geosphere, v. 19, p. 1128–1156, doi:10.1130/GES02611.1.

Seebeck, H., Van Dissen, R.J., Litchfield, N.J., Barnes, P.M., Nicol, A., Langridge, R.M., Barrell, D.J.A., Villamor, P., Ellis, S.M., and Rattenbury, M.S., 2022, New Zealand Community Fault Model - version 1.0: GNS Science Report, v. 2021/57, p. 97, doi:http://dx.doi.org/10.21420/GA7S-BS61.

Silva, V. et al., 2023, Global Seismic Risk Map:, doi:10.5281/ZENODO.8409623.

Stirling, M., Shaw, Bruce, Fitzgerald, M., and Ross, C., 2021, Selection and evaluation of magnitude–area scaling relations for update of the New Zealand National Seismic Hazard Model: University of Otago, 49 p.

Thingbaijam, K.K.S., Van Dissen, R.J., Shaw, B.E., and Gerstenberger, M.C., 2022, Average coseimic slip profiles:, doi:10.21420/S6ED-JN06.

United Nations Office for Disaster Risk Reduction, 2017, Words into Action Guidelines: National Disaster Risk Assessment- Tsunami hazard and risk assessment: UNISDR, https://www.preventionweb.net/files/52828_02tsunamihazardandriskassessment.pdf.

Van Dissen, R.J., Seebeck, H., and Henrys, S., 2023, Personal communication:

Wallace, L.M. et al., 2009, Characterizing the seismogenic zone of a major plate boundary subduction thrust: Hikurangi Margin, New Zealand: Geochemistry, Geophysics, Geosystems, v. 10, p. n/a-n/a, doi:10.1029/2009GC002610.

Wallace, L.M., 2020, Slow Slip Events in New Zealand: Annual Review of Earth and Planetary Sciences, v. 48, p. 175–203, doi:10.1146/annurev-earth-071719-055104.

Wallace, L.M., Beavan, J., McCaffrey, R., and Darby, D., 2004, Subduction zone coupling and tectonic block rotations in the North Island, New Zealand: Journal of Geophysical Research: Solid Earth, v. 109, doi:10.1029/2004JB003241.

Williams, C.A., Eberhart-Phillips, D., Bannister, S., Barker, D.H.N., Henrys, S., Reyners, M., and Sutherland, R., 2013, Revised interface geometry for the Hikurangi Subduction Zone, New Zealand: Seismological Research Letters, v. 84, p. 1066–1073, doi:10.1785/0220130035.

Youngs, R.R. et al., 2003, A Methodology for Probabilistic Fault Displacement Hazard Analysis (PFDHA): Earthquake Spectra, v. 19, p. 191–219, doi:10.1193/1.1542891.

FIGURE CAPTIONS

Figure M1. Schematic coastal coseismic vertical deformation and possible impacts. A) Pre-earthquake landscape and infrastructure. B) Post-earthquake landscape and effects after coseismic uplift (relative sea level fall). C) Post-earthquake landscape and effects after coseismic subsidence (relative sea level rise). In B-C, Black solid lines are the post-earthquake surface, grey solid lines are the pre-earthquake surface, and the dashed blue line is the former sea level location, relative to the landscape.

Figure 2. Study area location and tectonic context. A) The Wellington Region occupies the transition from Hikurangi subduction convergence in the north to a continental transform plate boundary to the south. The Community Fault Model (CFM) (Seebeck et al., 2022) is a simplified network of on- and offshore faults used in the NZ NSHM 2022. B) Study area with displacement sites used in modelling (white circles) and fault sections used in the elastic dislocation models (grey lines). The dashed grey line is the extension of the Palliser-Kaiwhata fault used in Alt. Fault 1 and 2 Meshes. C) Cross-sections of the fault models used in this study and the differences

in dip-slip components across key structures. Only one subduction interface model is ultimately used, but three crustal fault models test how uncertainty in fault geometry may affect displacement probability results. WHV=Wellington-Hutt Valley fault; W=Wairarapa fault; PK=Palliser-Kaiwhata fault.

Figure 3: Methodology overview of the PCDHM developed in this study. The majority of the input data are derived from the NZ NSHM 2022 logic tree branches and solutions. The orange rounded boxes represent the outputs or products at each step and the teal boxes are the key data inputs to produce a weighed mean hazard curve for one fault source model. The grey boxes are alternative parameters that can be used instead of the teal box in the same row; these parameters were also investigated but produce different results.

Figure 4: Examples of single earthquake rupture slip and vertical surface deformation. A) Crustal fault earthquake scenario on the CFM Mesh, showing slip and coseismic displacement. Grey rectangles show all fault sections included in the SRM rupture scenario, with red lines indicating the surface trace. Colored polygons indicate the fault sections used in the elastic dislocation models for this study. B) Earthquake scenario slip on the subduction interface (no dip modifications) and resulting coseismic displacement. The grey rectangles show all interface fault sections as used in the SRM. The rectangular patches must be converted to a triangular mesh to remove the gaps and overlaps between adjacent fault sections. The colored polygons indicate the discretized mesh fault sectioned used to calculate vertical displacement. In the right plots, vertical deformation contour intervals are 1 m; dark red solid lines > 0 m, grey dashed = 0 m, and solid blue lines < 0 m.

Figure 5. Hazard curves for a single branch of the subduction interface source model (no dip modifications, uniform slip). Each hazard curve shows the probability of exceeding a certain displacement threshold from subduction earthquakes. In general, subsidence hazard is greater at eastern sites and uplift hazard increases toward the Hikurangi trench in the east. The grey dashed lines show probabilities and minimum displacements depicted in Fig. 6. CBD = Central Business District.

Figure 6. Example of probabilities and minimum displacements at specific hazard curve values (see Fig. 5) for a single branch of the subduction interface source model. A) Displacements at the 10% and 2% probabilities of exceedance for each site. B) Probabilities of exceeding 0.2 m uplift or subsidence, rounded to the nearest percent.

Figure 7. Hazard curves for a single branch of crustal fault-only source model (CFM Mesh, uniform slip). Each curve shows the probability of exceeding a certain displacement threshold from crustal fault earthquakes. Site hazards vary depending on proximity to fault sources and the earthquake rates in the branch solution catalogue. The grey dashed lines show probabilities and minimum displacements depicted in Fig. 8.

Figure 8. Probabilities and minimum displacements at specific values on the hazard curves in Fig. 7. These values are from a single branch of a crustal-only source model (CFM mesh, uniform slip). A) Displacements are the 10% and 2% probabilities of exceedance for each site. B) Probabilities of exceeding 0.2 m uplift or subsidence, rounded to the nearest percent. For this

branch, the probabilities of uplift and subsidence vary based on local fault dip, rake, and earthquake rate.

Figure 9. PCDHM results from all branches of a crustal fault-only source model (CFM Mesh, uniform slip). A) Hazard curves from all branches in the source model logic tree. Shaded area is the range of single branch curves. The weighted mean is based on branch weights from the SRM (Gerstenberger et al., 2022a, 2024a). The probabilities of exceedance shown are for subsidence (i.e., the subsidence thresholds are negative displacements). B) Subsidence values at the 2% probability of exceedance (dashed line in A). C) The probability of exceedance at the 0.2 m subsidence threshold (dash-dot line in A). Error bars in parts B-C are the maximum and minimum branch values shown in part A.

Figure 10. PCDHM result sensitivity to dip changes on the subduction interface source model. A) Subsidence hazard curves from three subduction interface source models with different overall dips. Shaded regions are the range in branch values for each source model and solid lines are the weighted means. B) Minimum subsidence at the 2% probability of exceedance. C) The probability of exceedance at the 0.2 m subsidence threshold. Error bars in parts B-C are the range in branch values shown in part A. Subduction interface dip has a negligible effect on the weighted mean probabilities for displacement hazard.

Figure 11: Effect of crustal fault source model geometry on PCDHM. A) Subsidence hazard curve comparison for all sites. Solid lines for each fault model are the weighted mean of all branches and shaded envelope shows the branch result range. B) Minimum subsidence at 2%

probability of exceedance for all three fault models. C) The probability of exceedance at the 0.2 m subsidence threshold. Error bars in B-C show the range in branch results (shaded polygons) shown in A.

Figure 12: Example of how small changes to the fault mesh geometry impacts the PCDHM results at a single location: Porirua (see Fig. 2 for location). A) Location map of Porirua and modelled fault sections (red lines) used in the PCDHM. B) Schematic cross-section of the modelled Ohariu Fault for three different crustal fault meshes. The adjacent faults (red ticks) have the same geometry as the Ohariu Fault but are not depicted. Only the dip-slip component is shown since strike-slip does not contribute significantly to vertical deformation. C) Probabilities of exceeding 0.2 m uplift or subsidence. The alternative meshes (Alt. Fault 1 and 2) more likely to cause vertical deformation than the CFM Mesh. D) Minimum displacements at the 10% and 2% probability of exceedance. All source models use uniform slip. points and bar values in C-D are the weighted mean values of all branches; error bars show the branch range.

Figure 13: Effect of slip distribution on subsidence hazard for the CFM Mesh source model. The uniform or tapered slip applies to a single earthquake rupture within a branch; the values here are weighted means and branch ranges. A) Hazard curves for subsidence thresholds at all the sites. Solid lines are the source model weighted mean; shaded envelope is the branch range. B) Minium subsidence at 2% probability of exceedance. C) Probability of exceeding 0.2 m subsidence. The overall impact to vertical displacement hazard from slip distribution is minor.

Figure 14. The influence of crustal fault branch parameters on PCDHM results at three sites (additional sites available in supplement). All results are for the CFM Mesh with uniform slip. Branch parameters are A) time dependence, B) crustal deformation model, C) non-stationary moment-rate scaling parameter (S-value) and D) magnitude-frequency distribution. The effects are different for each individual fault source and thus vary from site to site, but some branch parameters have greater effects than others. Teal, purple, and orange-lines are hazard curves from individual branches in a source model and the thick blue line is the weighted mean subsidence hazard curve of all branches.

Figure 15. Relative contributions to PCDHM results from the crustal Alt. Fault 2-only, subduction-only, and crustal-subduction-combined source fault models in 100 years. Both the crustal (Alt. Fault 2 Mesh fault source) and subduction fault source (unmodified dip) have uniform slip distributions. A) Hazard curves for subsidence thresholds at all sites; solid lines are the weighted mean of all branches in the fault model logic tree, shaded envelopes are the branch range. B) Minimum subsidence at the 2% probability of exceedance (POE). C) POE for the 0.2 m subsidence threshold. For B- C, the bars and markers represent the weighted mean; error bars show the range in branch results.

Figure 16: Schematic block diagram showing weighted mean PCDHM results of a combination (crustal fault CFM mesh and subduction interface) source model in the context of tectonic setting and site location. A) Minimum vertical displacements at the 2% Probability of exceedance (red is uplift, blue is subsidence). Sites “Wellington Airport” and “Seaview” have been removed for figure clarity but have similar results to adjacent sites. B) Probabilities at the 0.2 subsidence

threshold. These results only show the weighted mean value and do not include the full branch range (i.e., error bars) shown in previous figures.

TABLE CAPTIONS

Table 1. Glossary of terms and initialisms used throughout this manuscript.

TABLE 1. GLOSSARY OF TERMS

Term and abbreviation	Definition and chapter usage
Earthquake rupture scenario	Hypothetical but geologically plausible synthetic earthquakes, as provided in the *New Zealand National Seismic Hazard Model 2022 (NZ NSHM 2022)* solutions. Each earthquake rupture scenario consists of a collection of ruptured *fault subsections*, average slip value, and an annual rate of occurrence. The annual rate of occurrence for an earthquake rupture scenario can be zero. The *earthquake rupture scenario* solutions (average slip, rate) differ between each *logic tree branch*.
Elastic dislocation model	A method for calculating coseismic surface displacement from hypothetical slip on a fault or faults. Displacements result from applying a specified slip amount and rake to a planar fault geometry in an elastic half-space (Okada, 1985). This study uses the method of Nikkhoo & Walter, (2015) for triangular slip surfaces.
Fault mesh	Collection of fault traces, subsurface geometries, and rakes that define either the crustal fault network or the subduction interface surface. These *fault meshes* are represented by triangular surfaces that are continuous along fault strike. The meshes are used as the *elastic dislocation model* sources. We tested three crustal *fault meshes* and three subduction interface *fault meshes*.
Source model	Defined set of variables and solutions used in the PCDHM. Variables include *SRM logic tree* (s), *fault mesh(es)*, and slip distribution(s). The *source model* can use crustal-only, subduction interface-only, or combined crustal-subduction interface fault meshes. The *logic tree branch* parameters and weights are defined by the *SRM*. The crustal fault slip distribution can be tapered or uniform; subduction interface slip is always uniform. The *source model* solutions are composed of hazard curves for each logic tree branch and a weighted mean hazard curve (across all branches in a *source model*).
Inversion Fault Model (IFM)	A method for determining the rate of earthquakes in the *NZ NSHM* from defined fault sources in the *SRM*. The *IFM* uses various geologic, geodetic, and model-based data constrains to invert annual rates for each *earthquake rupture scenario* in each branch of the *SRM* logic tree (Gerstenberger, Van Dissen, et al., 2022). The *IFM* is based on the Grand Inversion of the UCERF3 earthquake rupture forecast (Field et al., 2014).

Logic tree/ Logic tree branch	A logic tree defines the weights for different epistemic uncertainty parameters and provides a mean hazard estimate with confidence bounds . Each logic tree branch and resulting NZ NSHM solution represents a unique combination of the uncertainty parameters. The weights of different parameter options sum to one, and the final summed branch weights within the entire tree also sum to one. This study uses two different SRM logic trees that contribute to results for different source models: one for crustal faults and one for the Hikurangi subduction interface (Gerstenberger et al., 2024b).
New Zealand National Seismic Hazard Model 2022 (NZ NSHM 20222)	A probabilistic seismic hazard assessment (PSHA) for the country of Aotearoa New Zealand for the next 100 years (Gerstenberger et al. 2024a). The main components used in this study are from the *SRM* .
Probabilistic Coseismic Displacement Hazard Model (PCDHM)	A framework for estimating the probability of coseismic displacement at a site (or sites) from all possible earthquakes in a certain time period.
Probabilistic Seismic Hazard Assessment (PSHA)	A method for quantifying the probability of exceeding various seismic ground motion levels at a site (or sites) from all possible earthquakes in a certain time period. Necessary components in a *PSHA* include earthquake source and recurrence data (e.g., fault location, earthquake magnitude, earthquake rate) and site-specific data related to seismic attenuation.
Relative Sea-Level change	The net change in sea level resulting from changes in in land elevation, sea level, or both. Coseismic subsidence causes instantaneous relative sea-level rise and coseismic uplift causes instantaneous relative sea-level fall.
Seismicity Rate Model (SRM)	A model within the *NZ NSHM* that produces average slip and annual rate for each *earthquake rupture scenario* from the crustal and subduction interface fault sources. The SRM includes solutions for all branches in the source *logic trees* and defines branch weights.

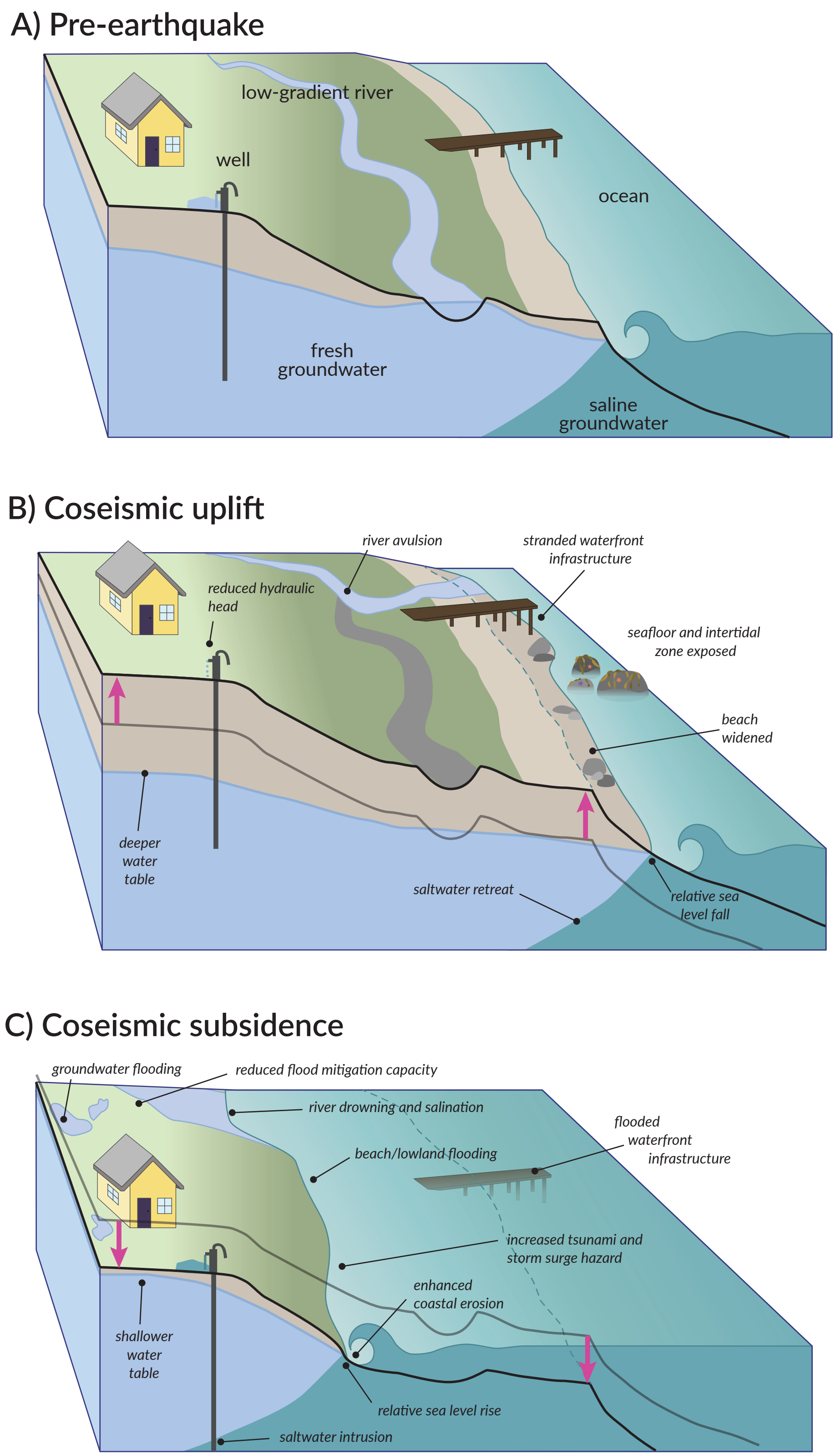

Figure 1

First Author: Delano
Manuscript number: TBD

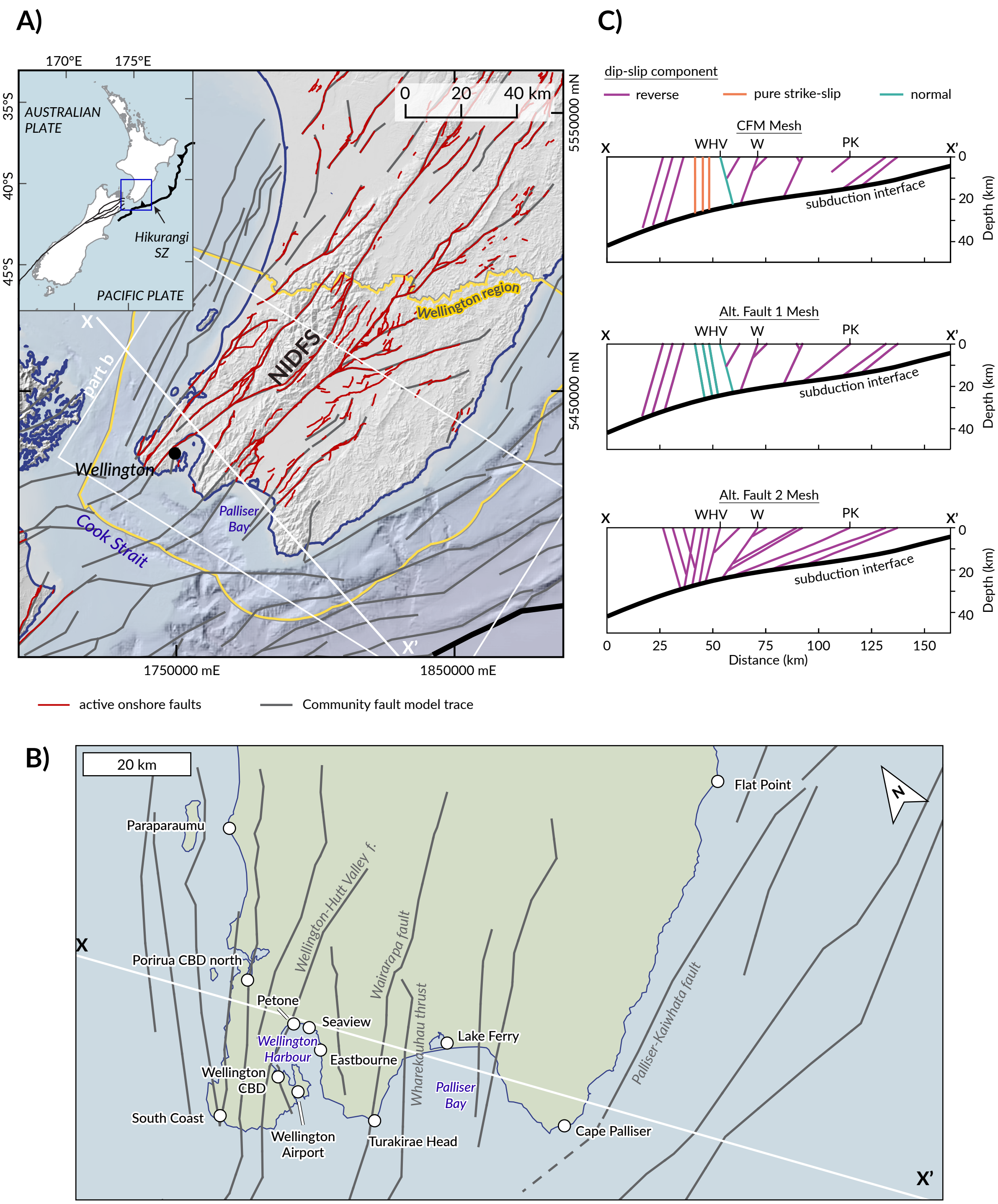

Figure 2

First Author: Delano
Manuscript number: TBD

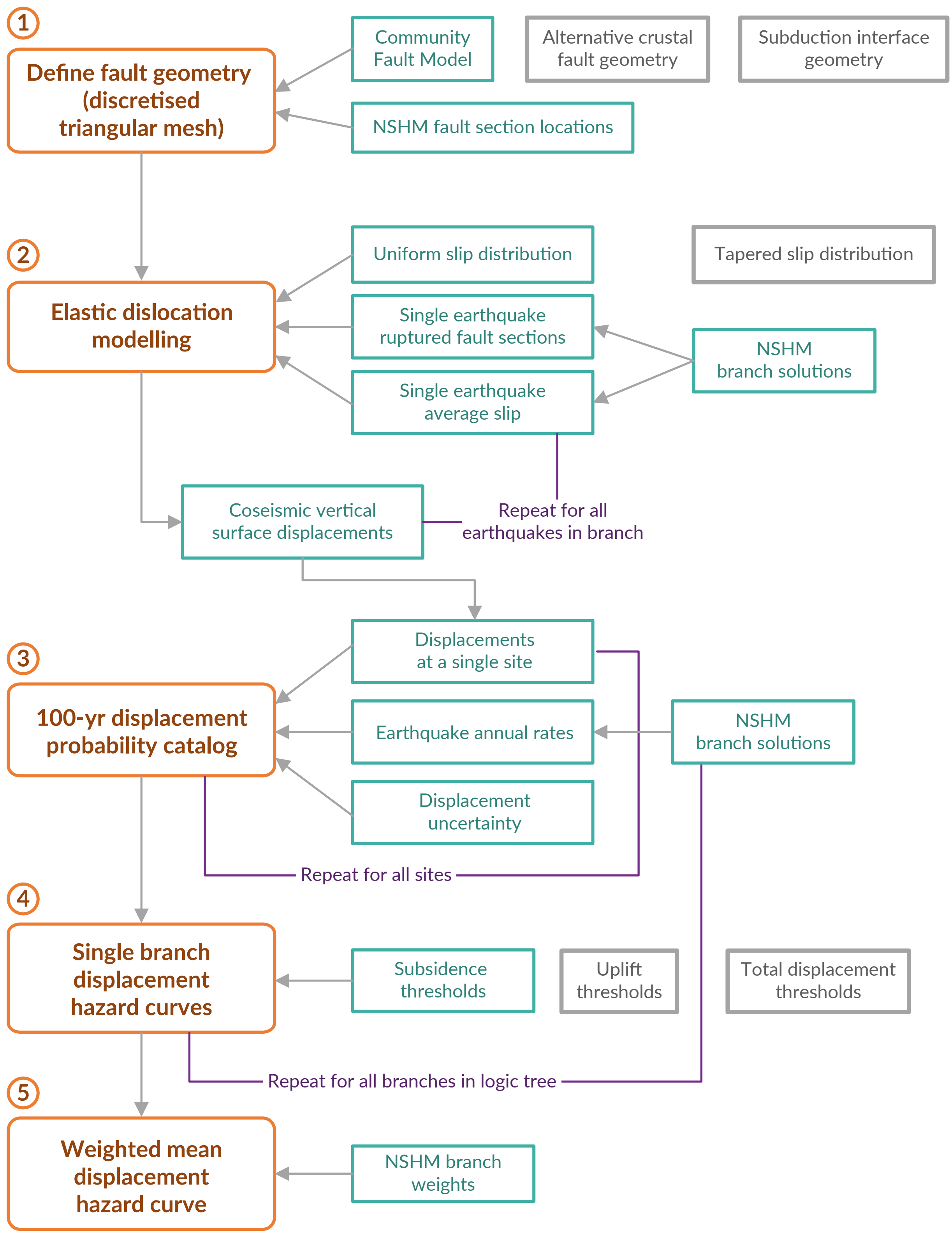

Figure 3

First Author: Delano
Manuscript number: TBD

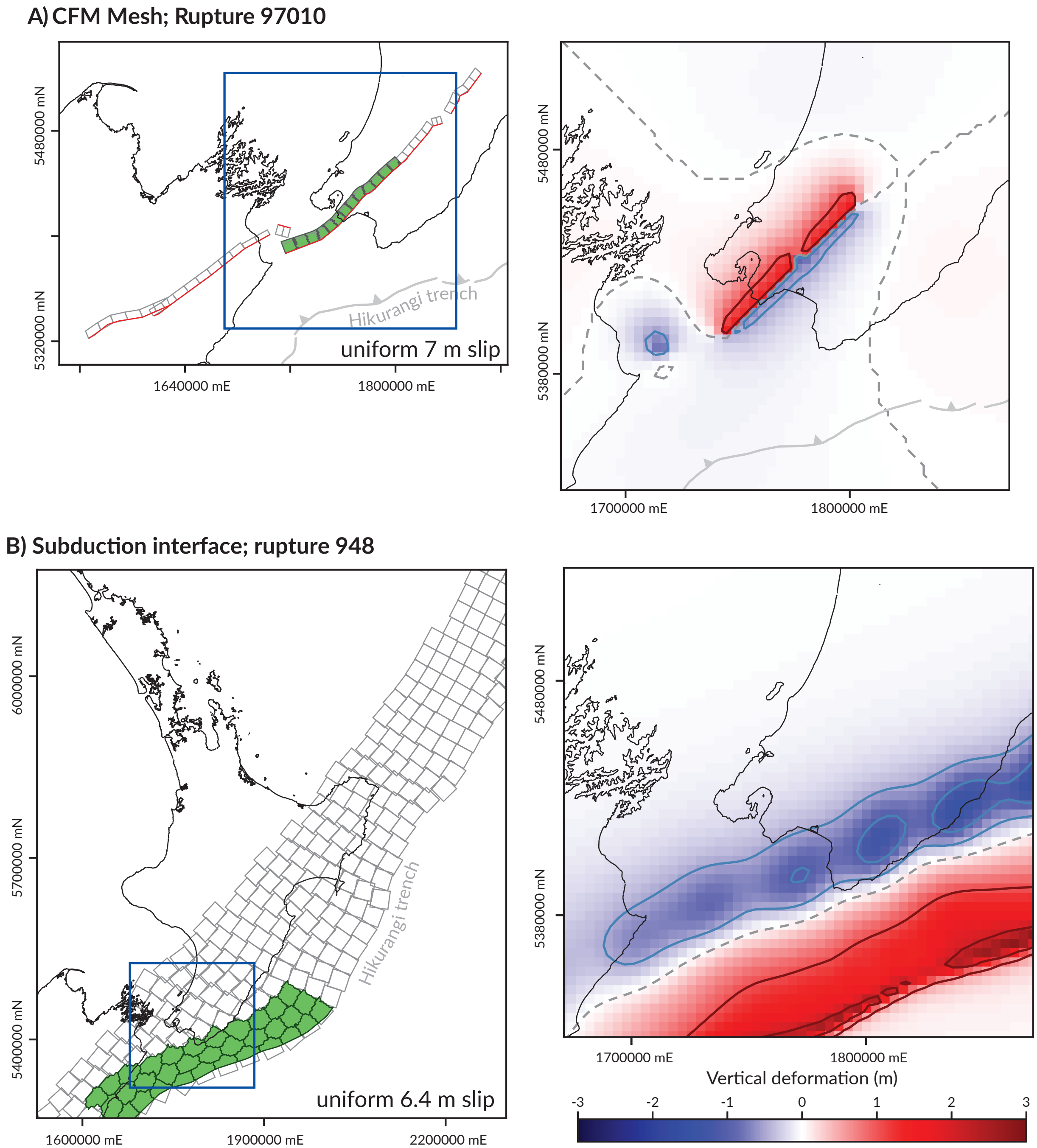

Figure 4

First Author: Delano
Manuscript number: TBD

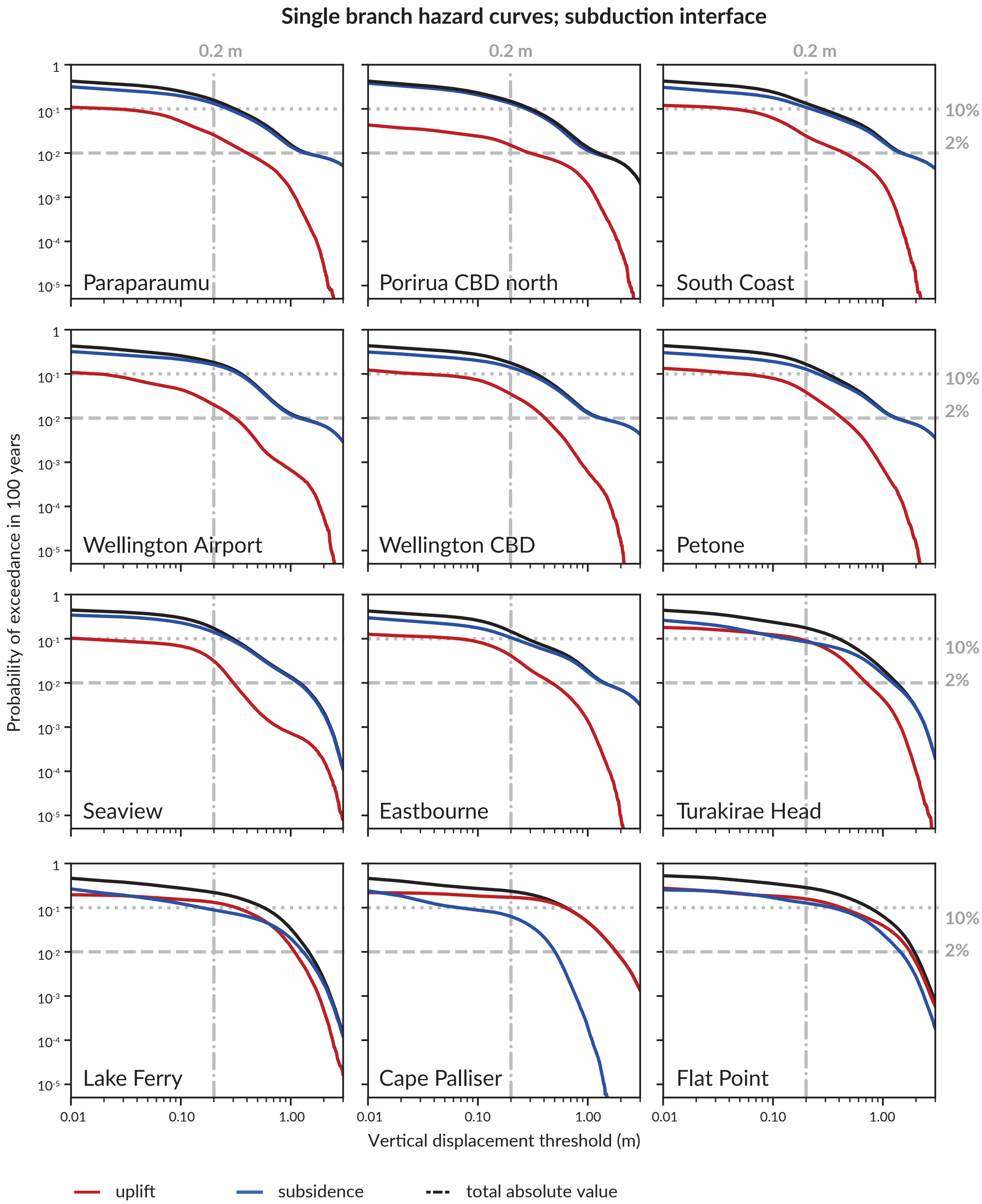

Figure 5

First Author: Delano
Manuscript number: TBD

Subduction interface single branch hazard results

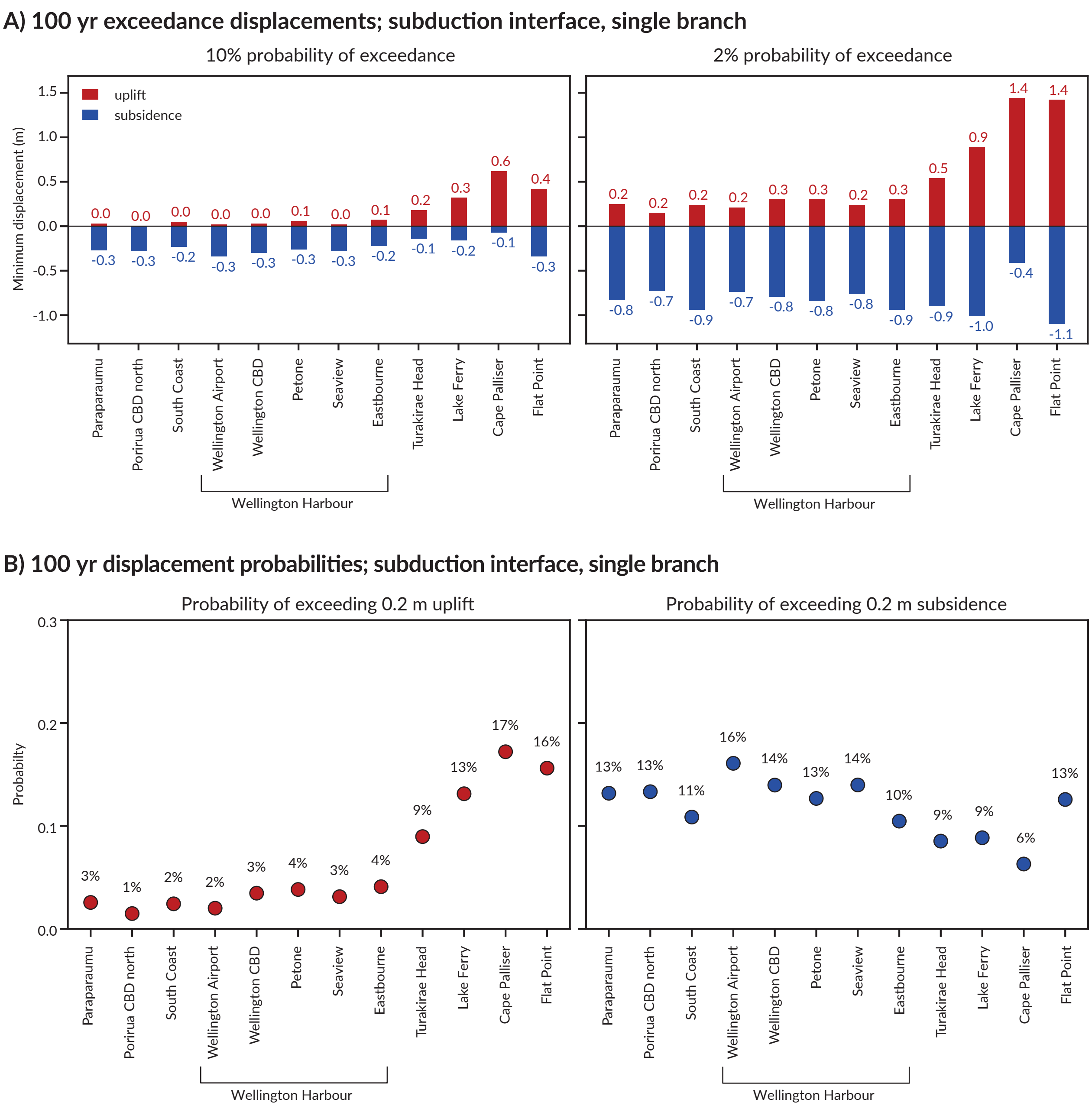

Figure 6

First Author: Delano
Manuscript number: TBD

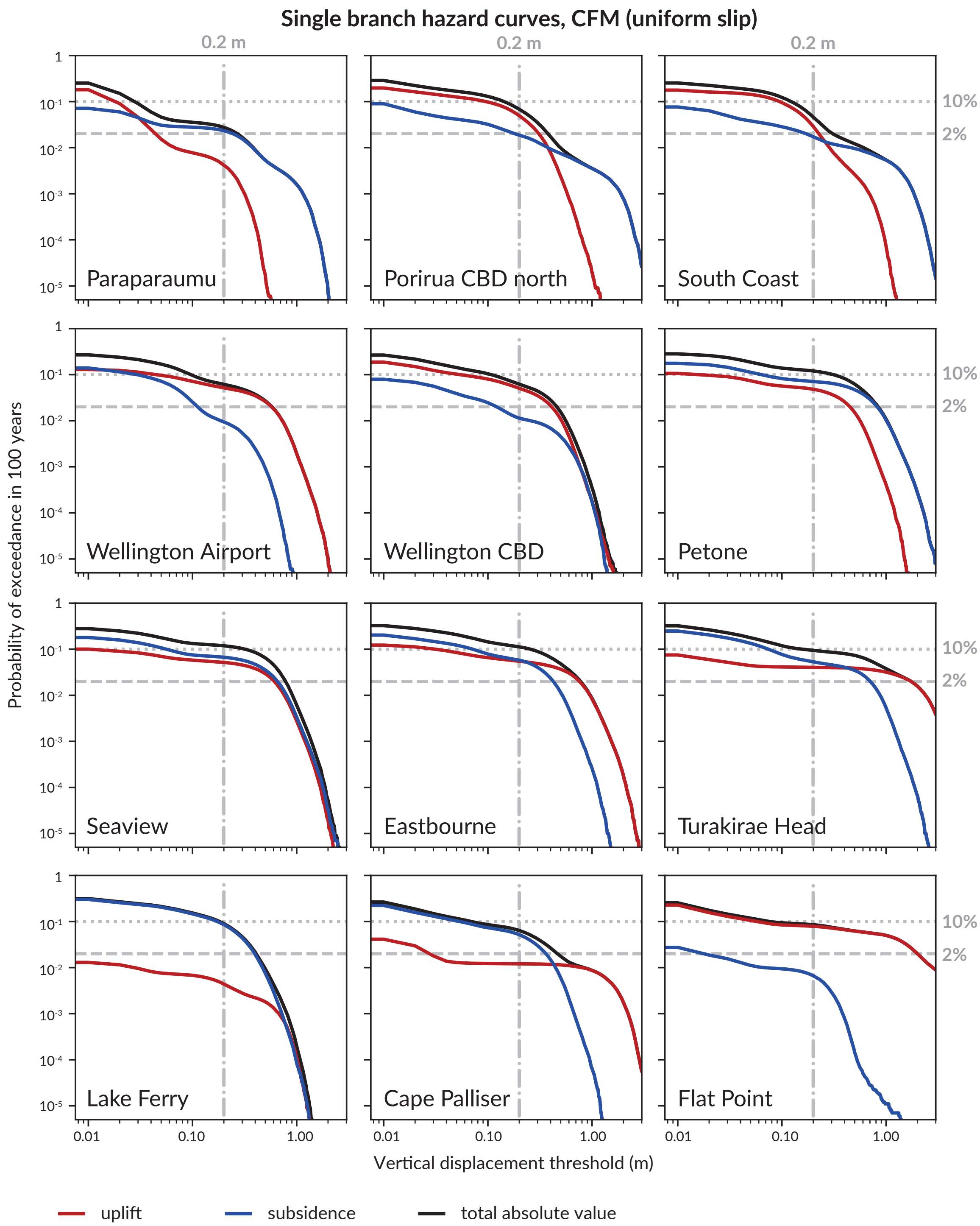

Figure 7

First Author: Delano
Manuscript number: TBD

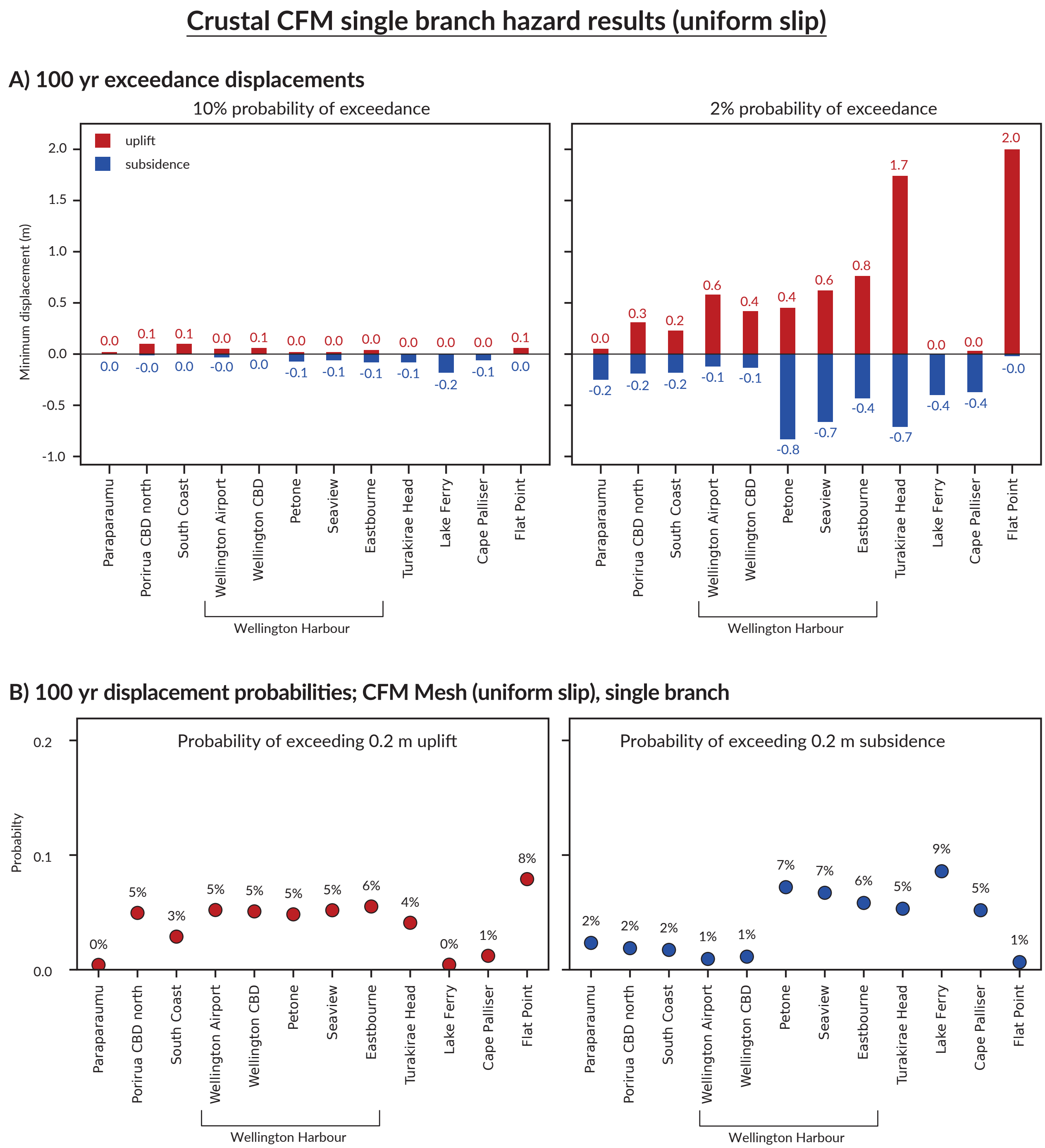

Figure 8

First Author: Delano
Manuscript number: TBD

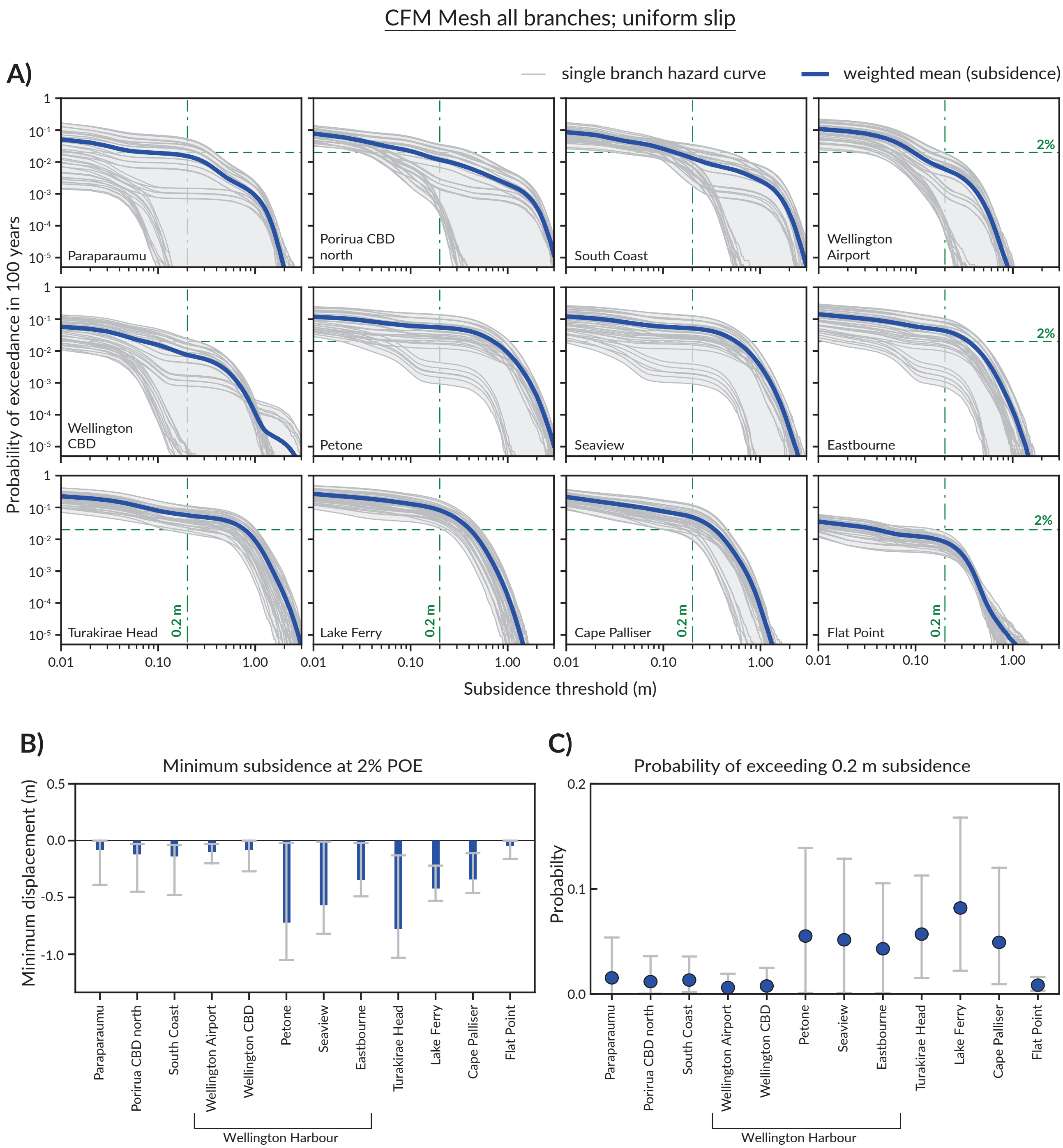

Figure 9

First Author: Delano
Manuscript number: TBD

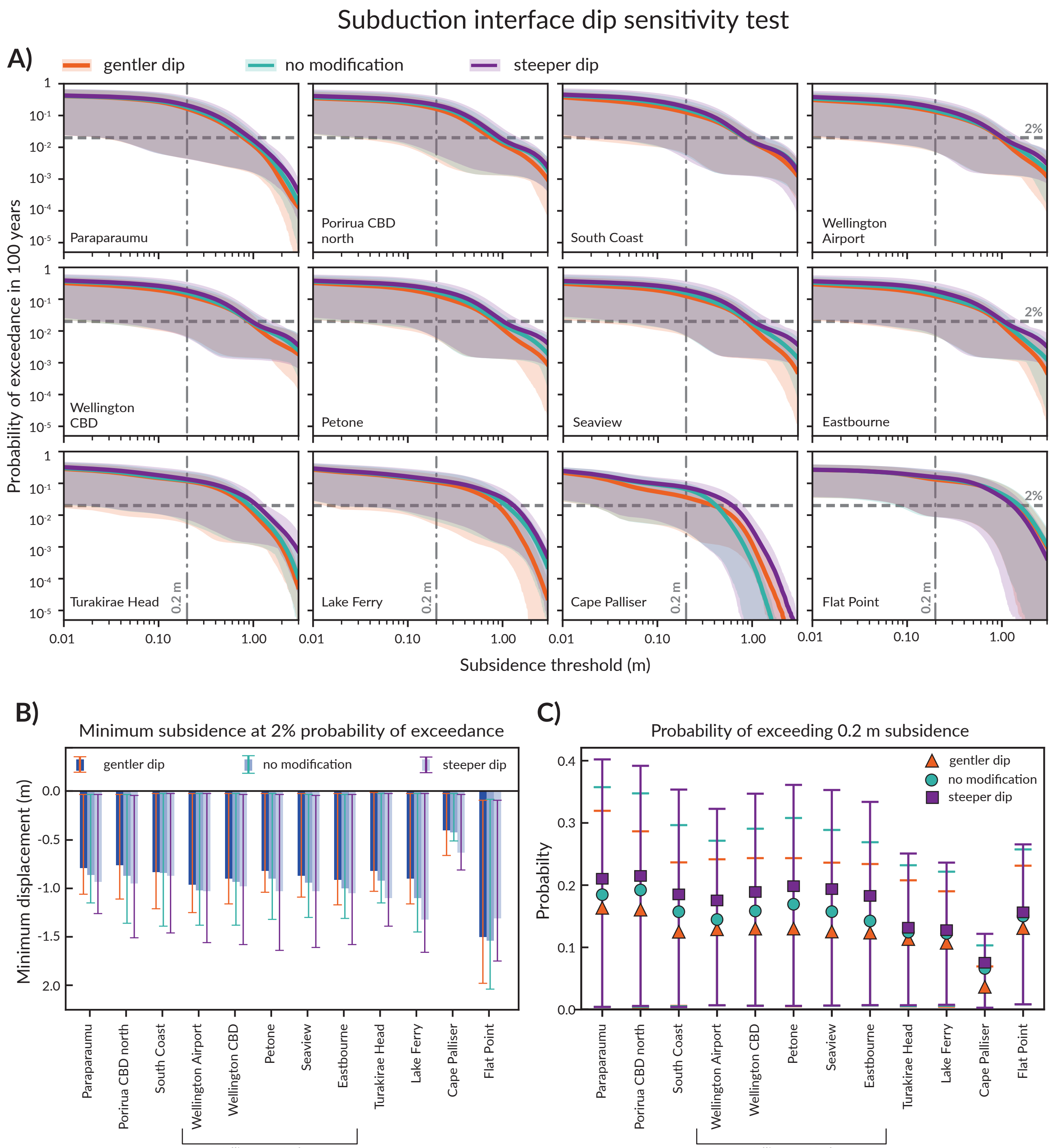

Figure 10

First Author: Delano
Manuscript number: TBD

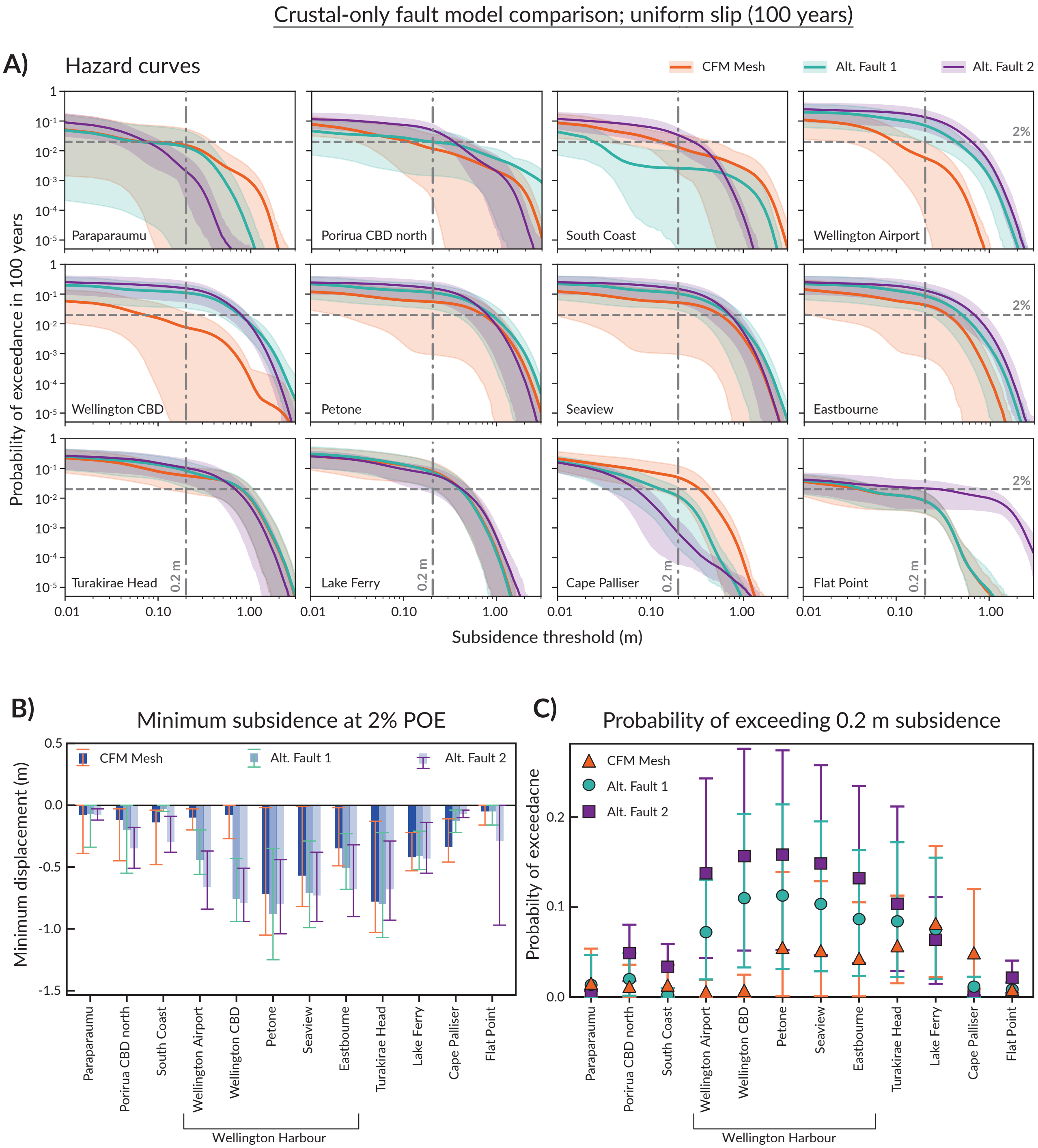

Figure 11

First Author: Delano
Manuscript number: TBD

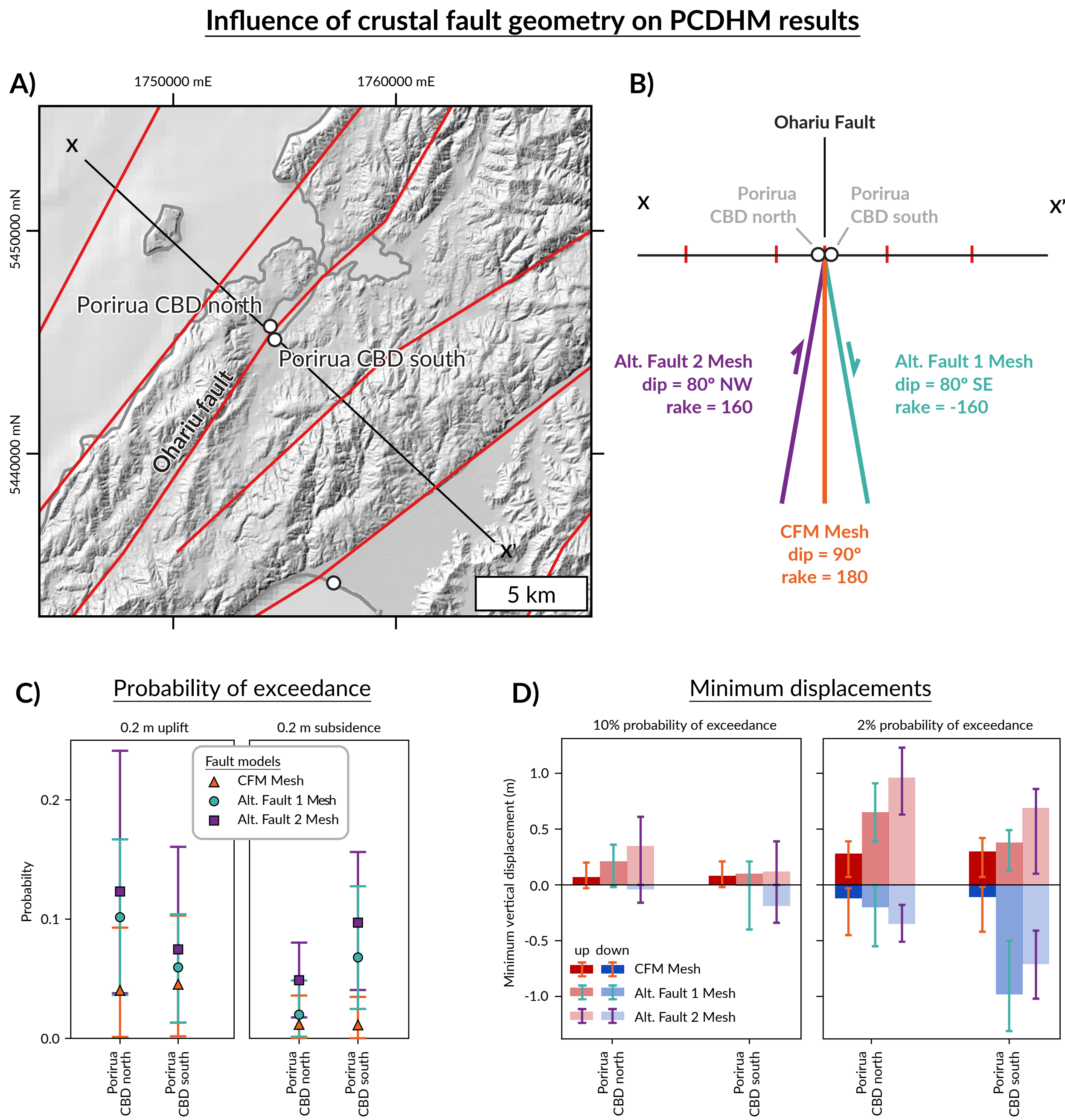

Figure 12

First Author: Delano
Manuscript number: TBD

Slip distribution sensitivity; CFM Mesh source model

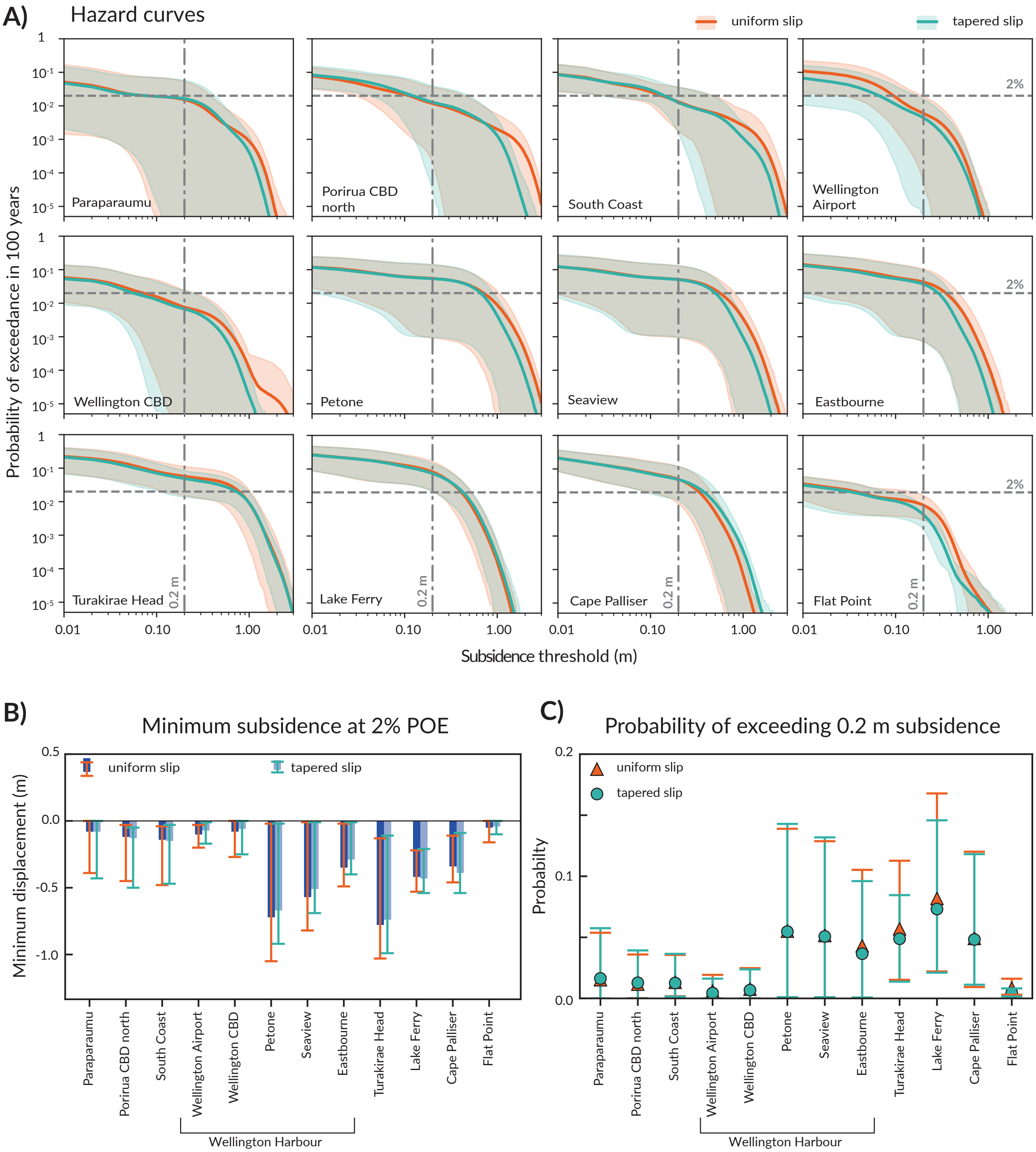

Figure 13

First Author: Delano
Manuscript number: TBD

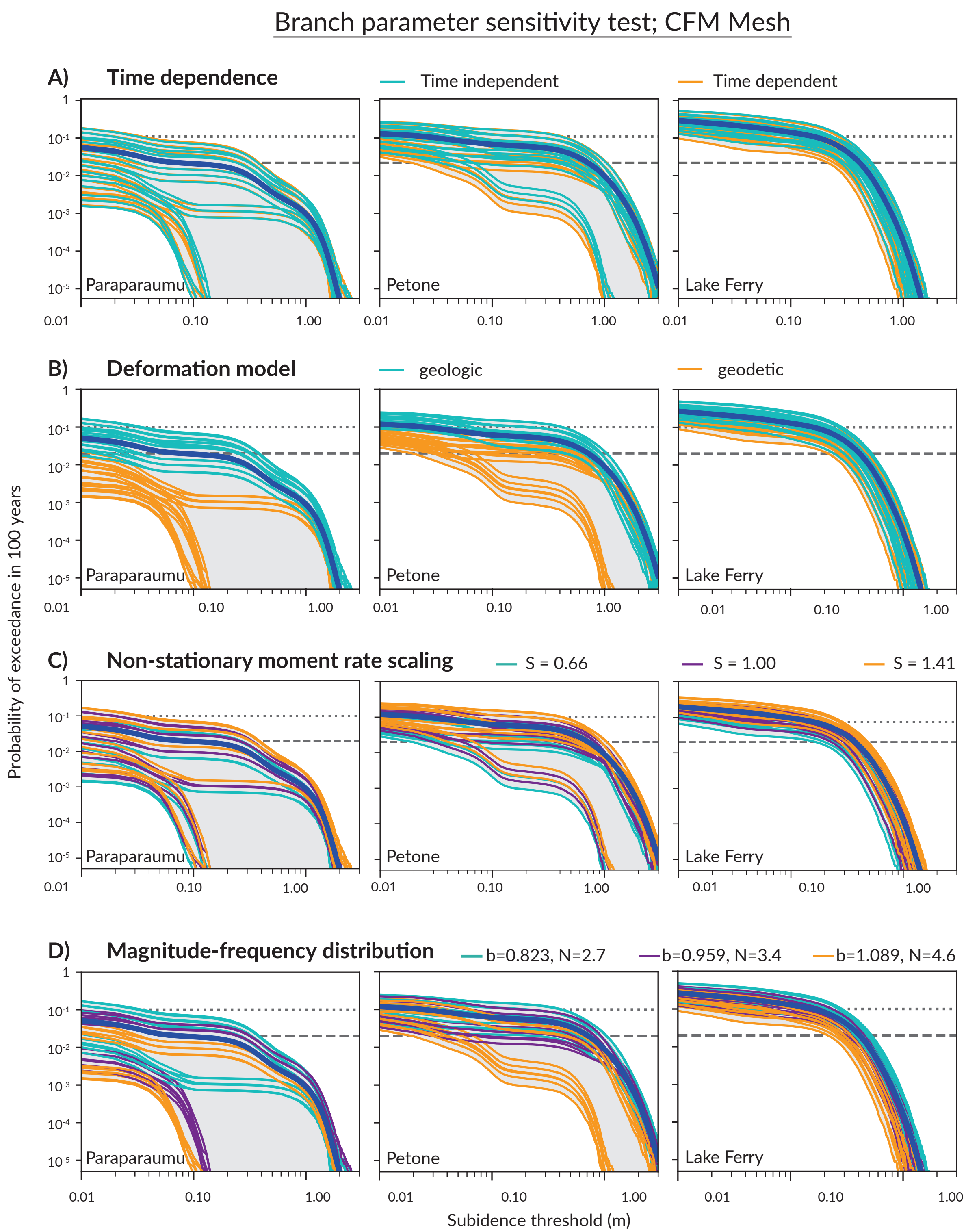

Figure 14

First Author: Delano
Manuscript number: TBD

Crustal fault (Alt. Fault 2) vs subduction interface hazard results

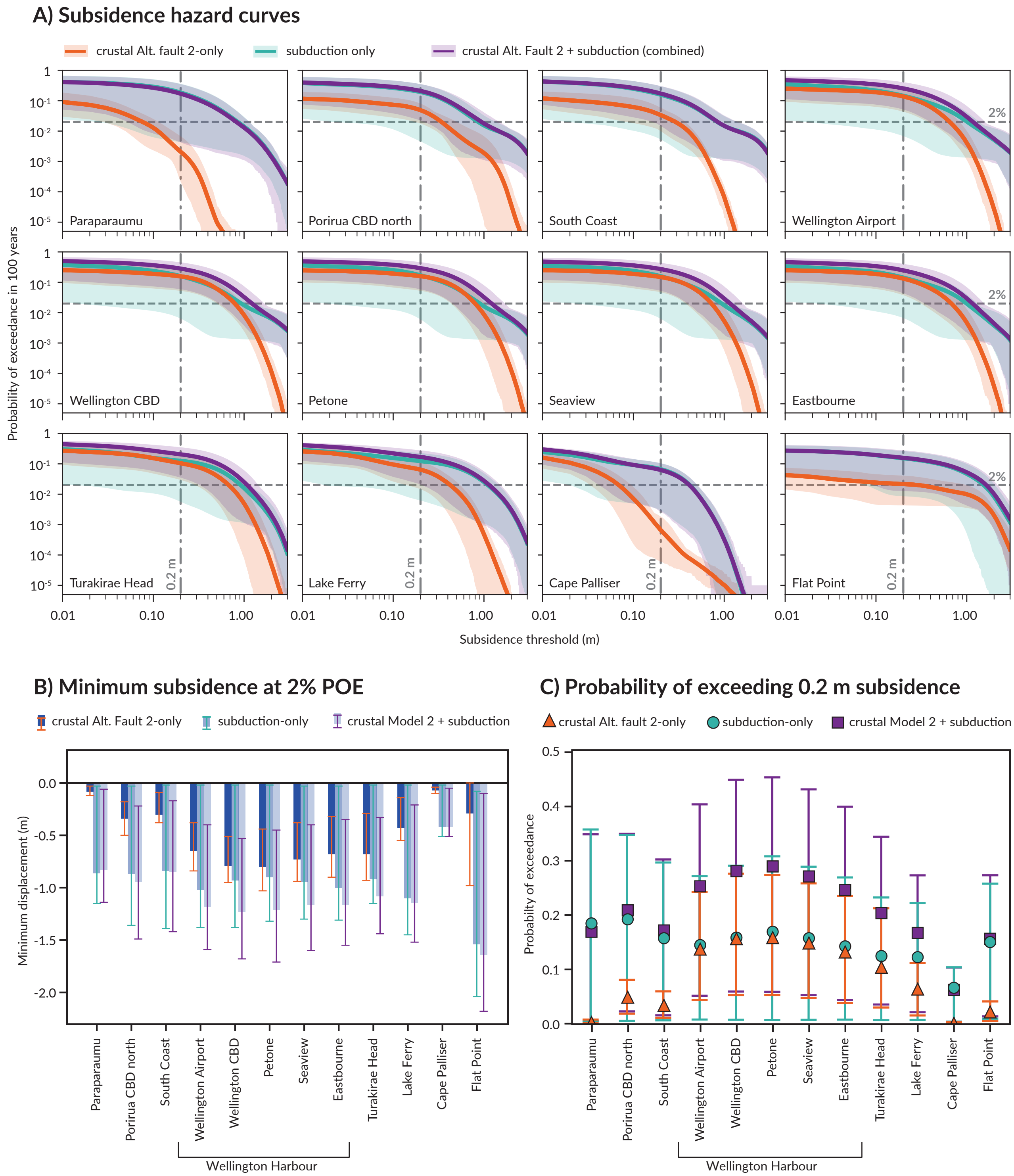

Figure 15

First Author: Delano
Manuscript number: TBD

Combined source: crustal (Alt. Fault 2) + subduction interface (100 yr)

A) Minimum displacements at 2% probability of exceedance

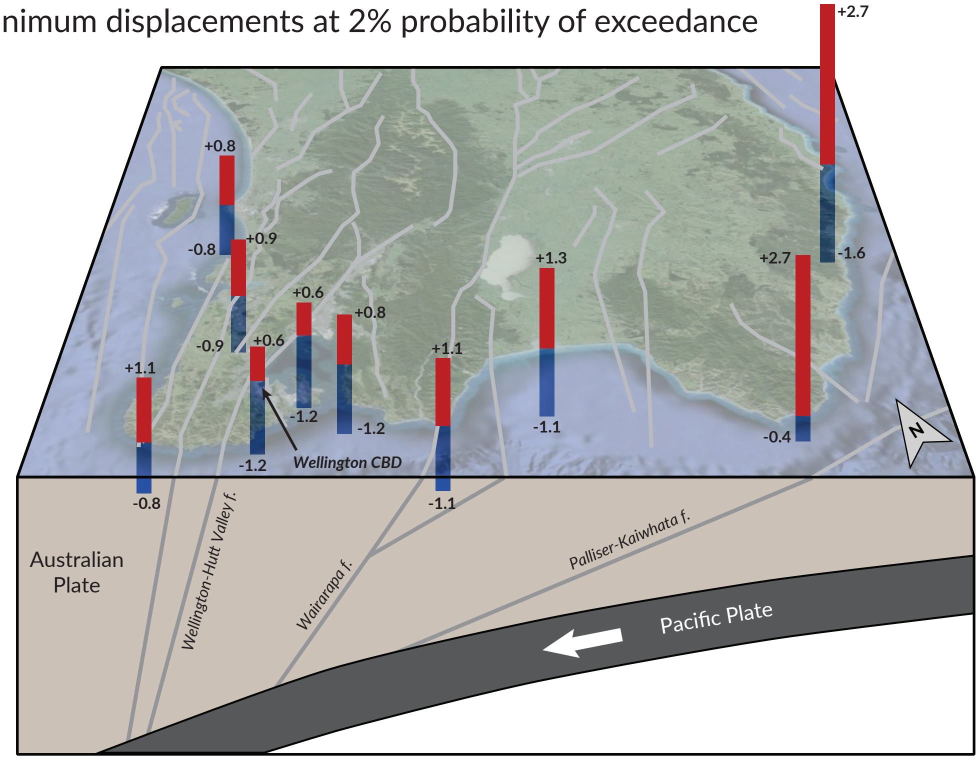

B) Probability of exceeding 0.2 m subsidence

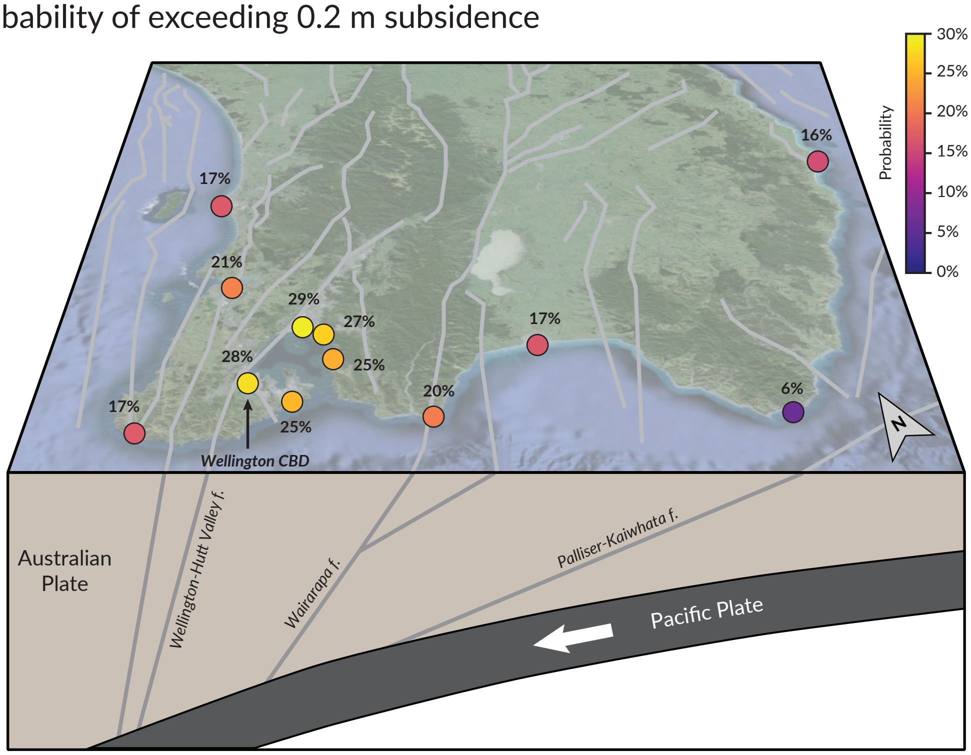

Figure 16

First Author: Delano
Manuscript number: TBD

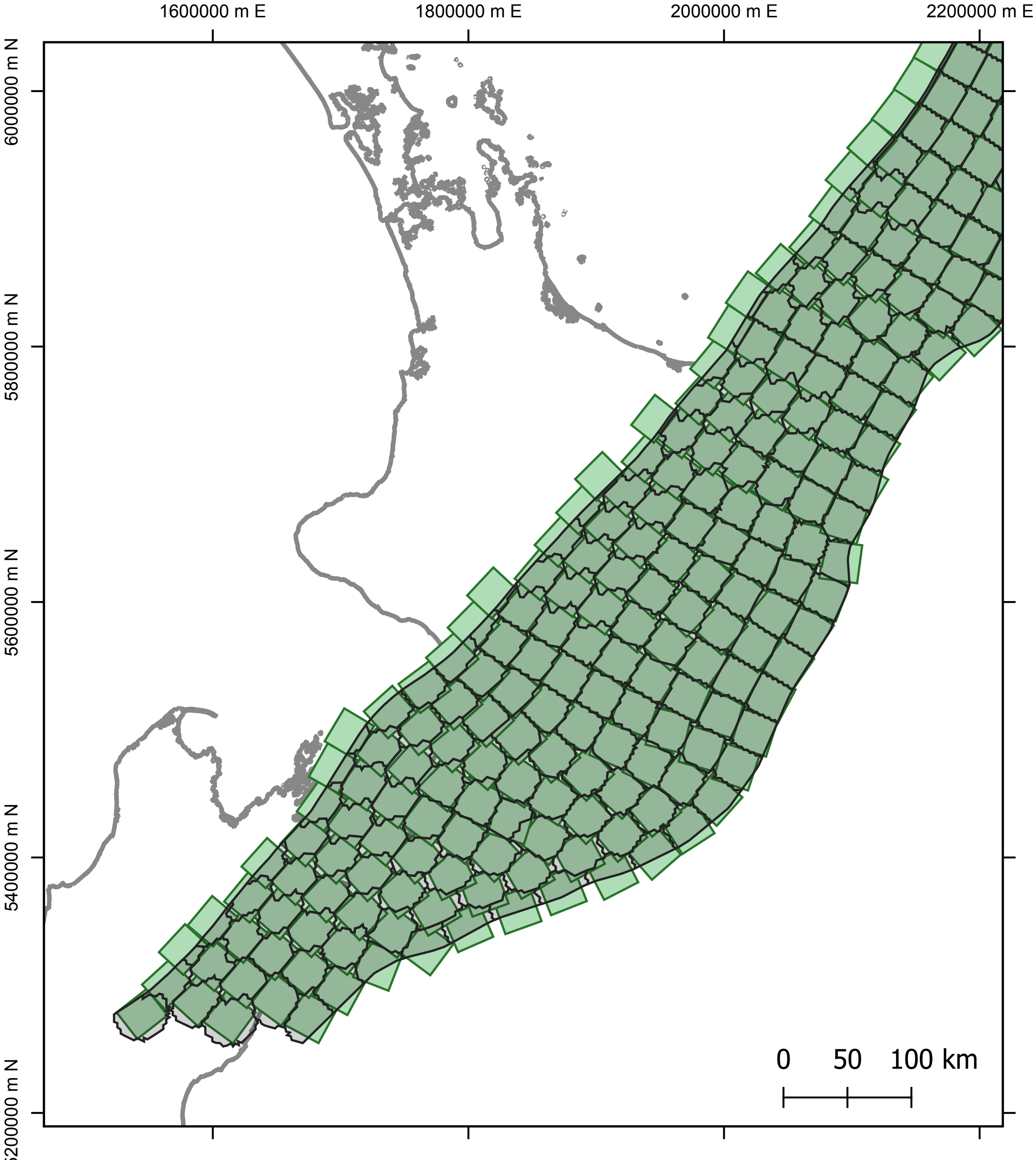

Figure S1: Discretized mesh vs regtangular patch for the Hikurangi subduction interface. The regtangular patches (green) are derived from the 2022 NZ NSHM fault sources. These patches are inadequate for calculating coseismic dipslacement because they overlap each other and have spatial gaps. The discretized mesh (grey/black polygons) is a continuous surface separated into discretized patches. Patches are discretized based on proximity to regular patch centroids and structural depth.

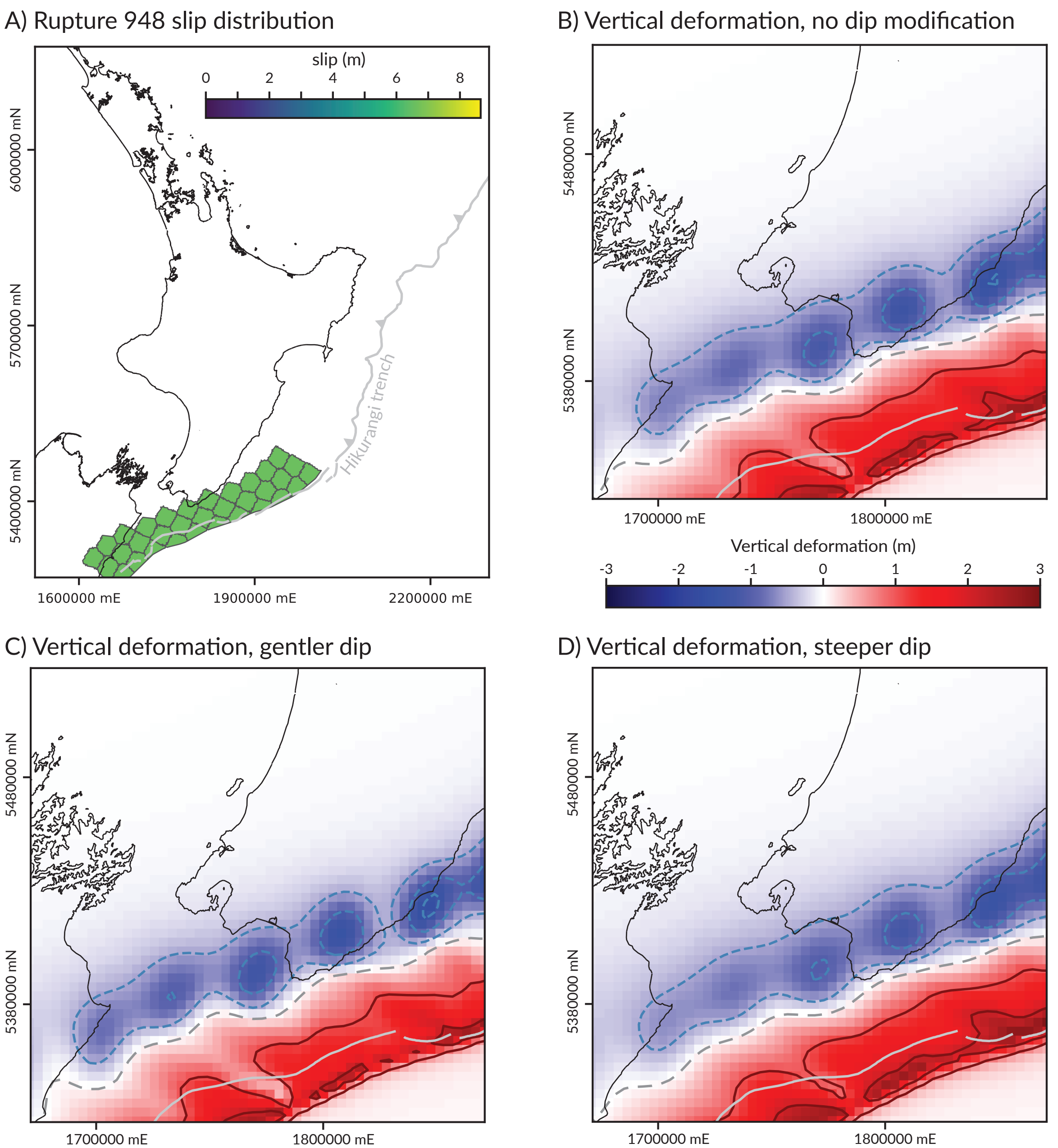

Figure S2: Examples of a subduction interface earthquake rupture scenario and deformation sensitivity to interface dip. (a) Uniform slip is applied to the discretized meshes, following the fault sections for rupture 948 in the SRM for a single branch. Teeth on the Hikurangi trench point downdip. Vertical deformation results shown from an interface with (b) with no dip modification, (c) an overall gentler dip, and (d) and overall steeper dip. Solid dark red and dashed blue lines indicate the 1 m contour intervals for uplift and subsidence, respectively. The dashed grey line is the 0 m contour. The effect of interface dip/depth changes in the amount modelled here are minor; we only use the “no modifications” mesh for the results.

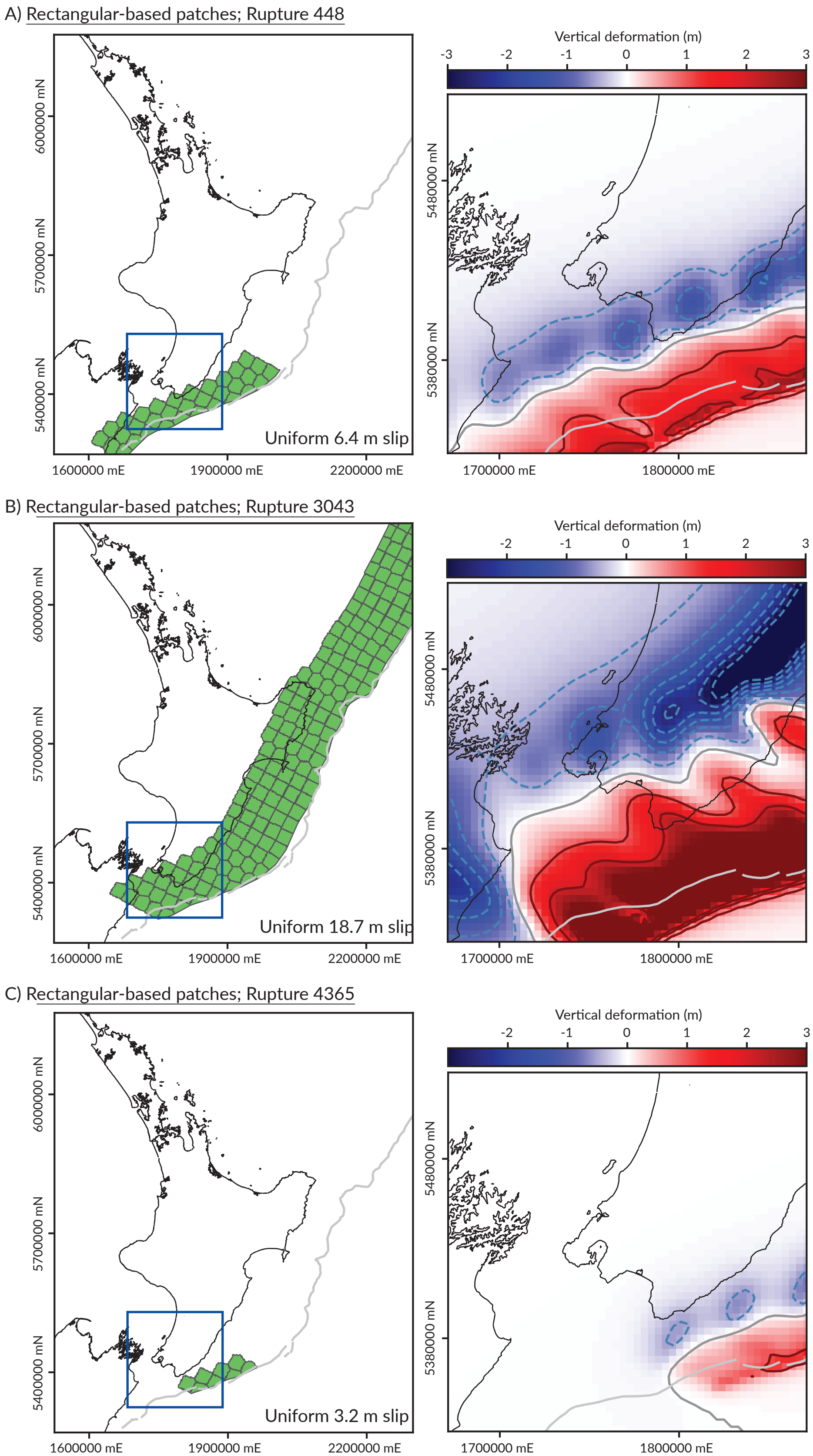

Figure S3: Example ruptures using subduction discretization following the NSHM rectangular fault patches. The resulting surface deformation pattern has a wavy pattern due to the shape of the slip patches at depth and variable slip rake between patches. It is pronounced where interface geometry/slip vector changes rapidly between patches near the southern interface. Results are from the MzMx branch suffix.

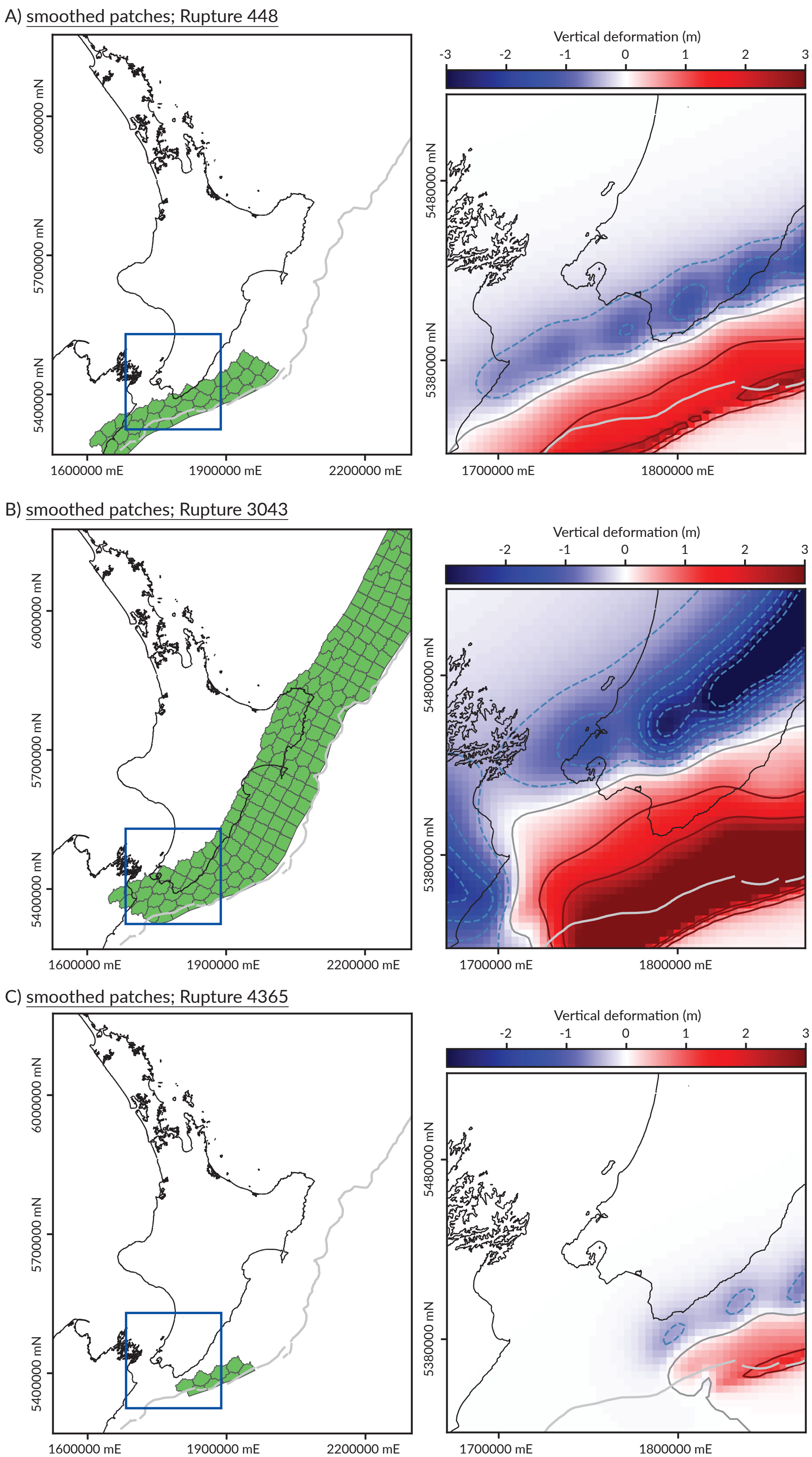

Figure S4: Example ruptures using subduction discretization that is more smoothed down-dip rather than folowing the rectangular NSHM fault section patches. The resulting durface deformation pattern is less “blobby” than in Figure S3.

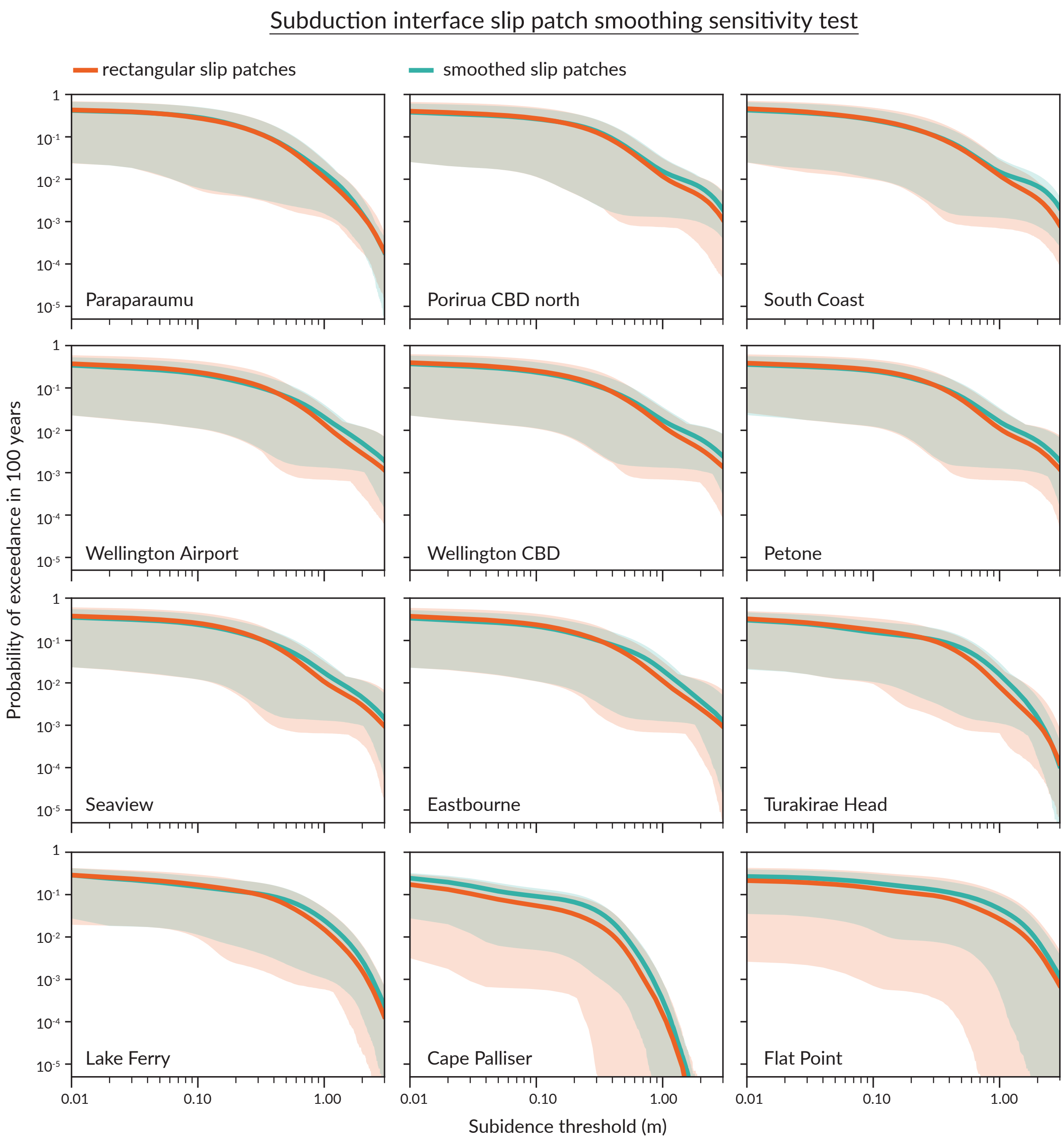

Figure S5: Hazard curve comparison between the rectangular-based slip patches and smoothed slip patches on the subduction interface. The impact to the final hazard curves is minimal, but is greatest at the eastern sites and at higher displacement thresholds.

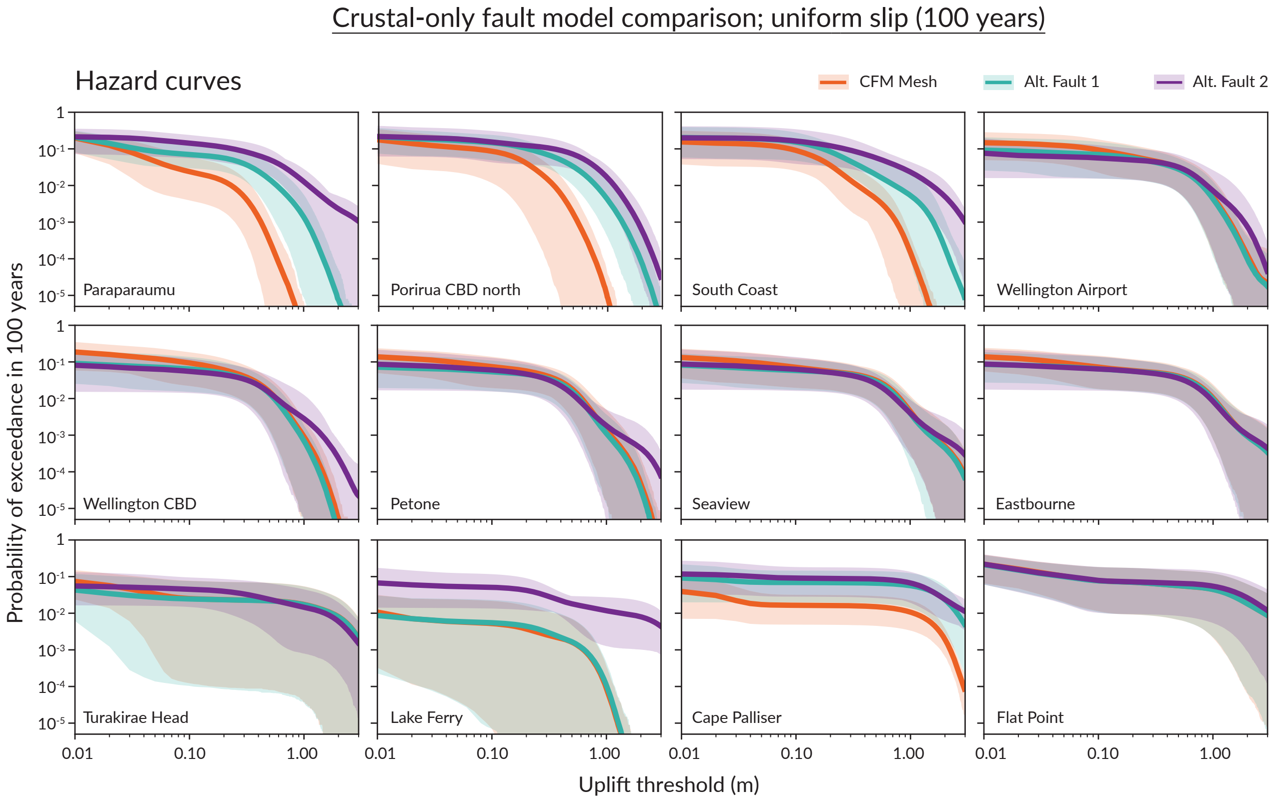

Figure S6: Uplift hazard curves for the three crustal-only source models (uniform slip). See Fig. 2 in main text and Table S2 for fault geometry differences. The gentler fault dips toward the east (closer to the Hikurangi trench) produce greater uplift probabilities at Lake Ferry and Cape Palliser. The differences between Alt. Fault 1 and 2 towards the western sites (e.g., Paraparaumu, Porirua, South Coast) are cased by opposite-dipping dip-slip faults.

Crustal fault source slip distribution sensitivity test: CFM Mesh

(a) Rupture scenario 97010 (uniform slip)

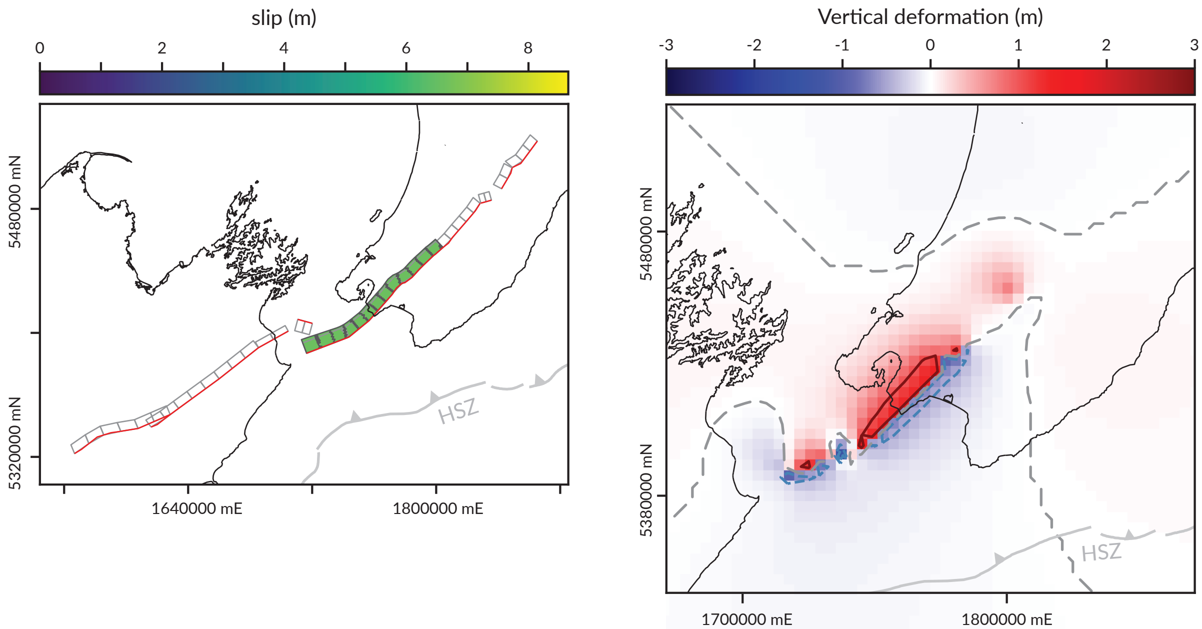

(b) Rupture scenario 97010 (tapered slip)

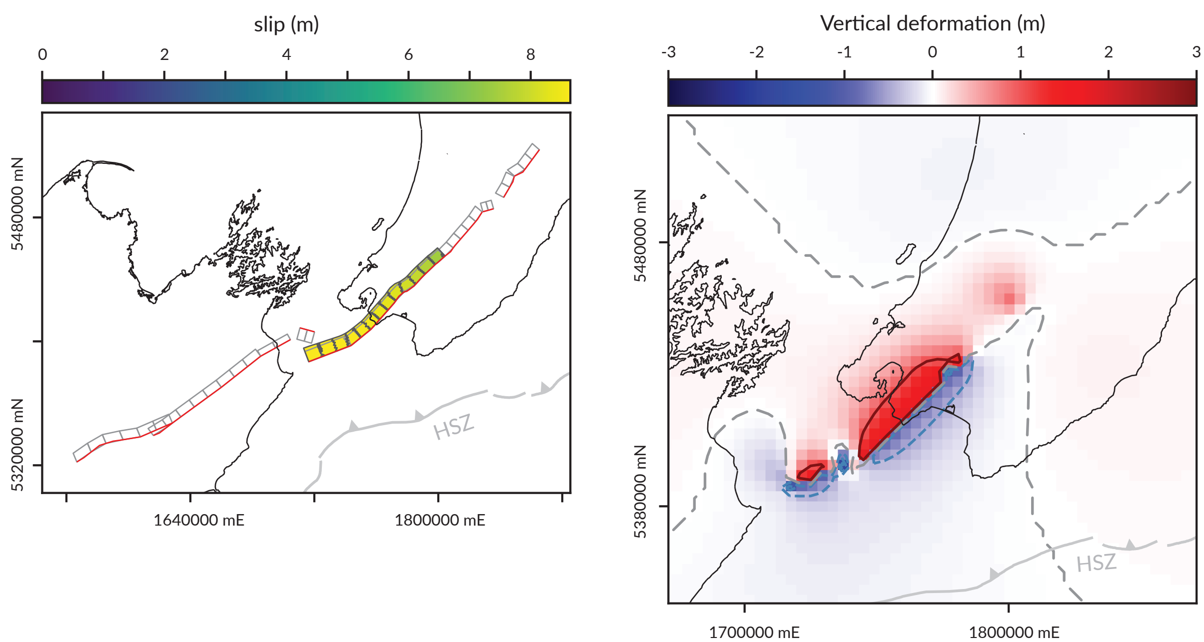

Figure S7: Examples of crustal fault earthquake rupture scenarios with (a) uniform slip and (b) tapered slip. For (b), slip is tapered along the entire rupture length. The left plots show the slip distribution used in the elastic dislocation models; the grey rectangles indicate the fault sections from the NZ NSHM that compose the entire earthquake rupture scenario; the black-outlined coloured polygons show the discretised mesh sections applied in the elastic dislocation, coloured by slip amount; and the red lines show the surface trace of the fault sections. In the right plots, the solid dark red, dashed grey, and dashed blue lines indicate the +1, 0, and -1 m vertical displacement contours, respectively. HSZ = Hikurangi Subduction Zone.

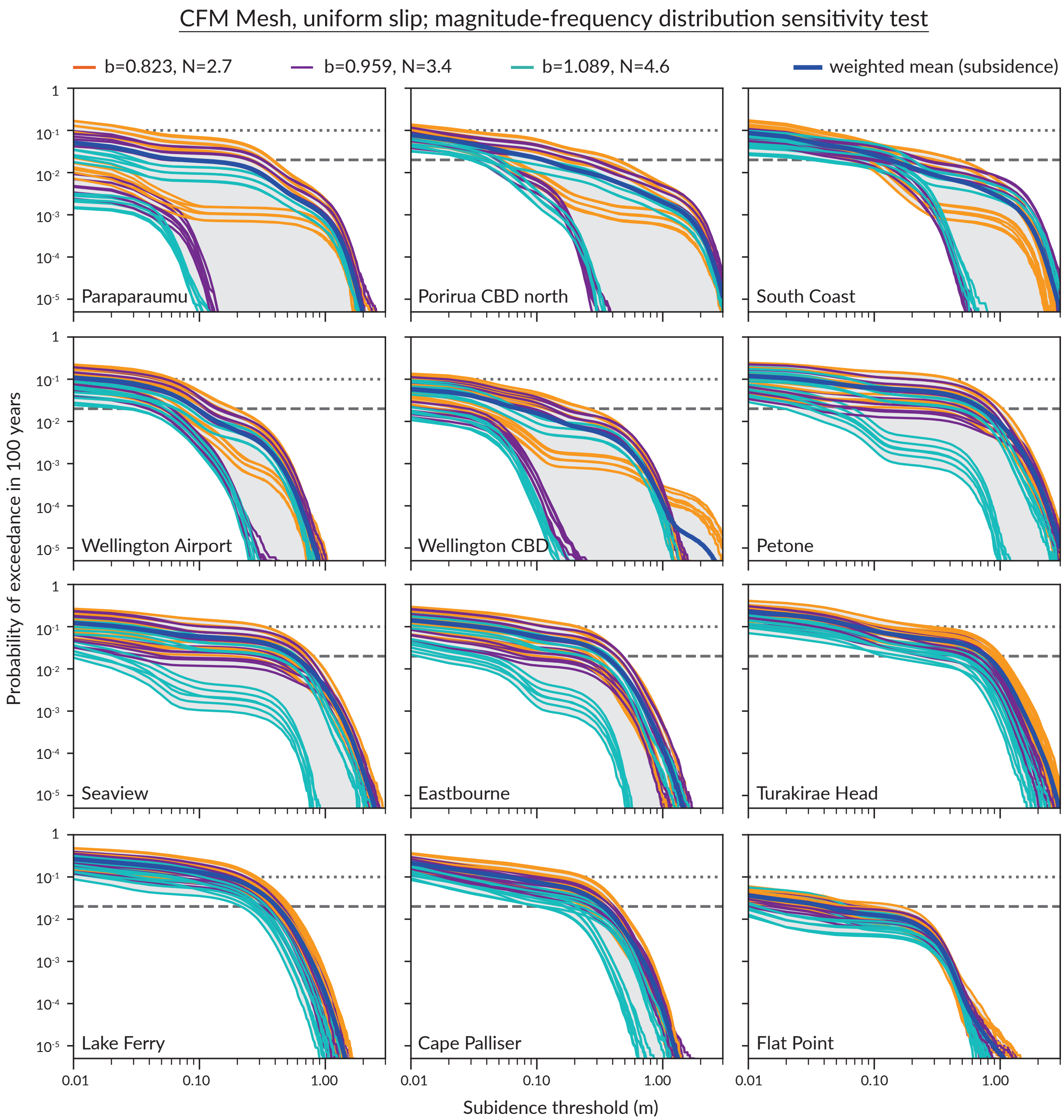

Figure S8: Magnitude frequency distribution parameter sensitivity test for a crustal-only source model (CFM Mesh, uniform slip). Branches with lower b- and N-values produce higher probabilities than branches with higher b- and N-values. Teal, purple, and orange lines are hazard curves from individual branches and the thick blue line is the weighted mean hazard curve of all branches.

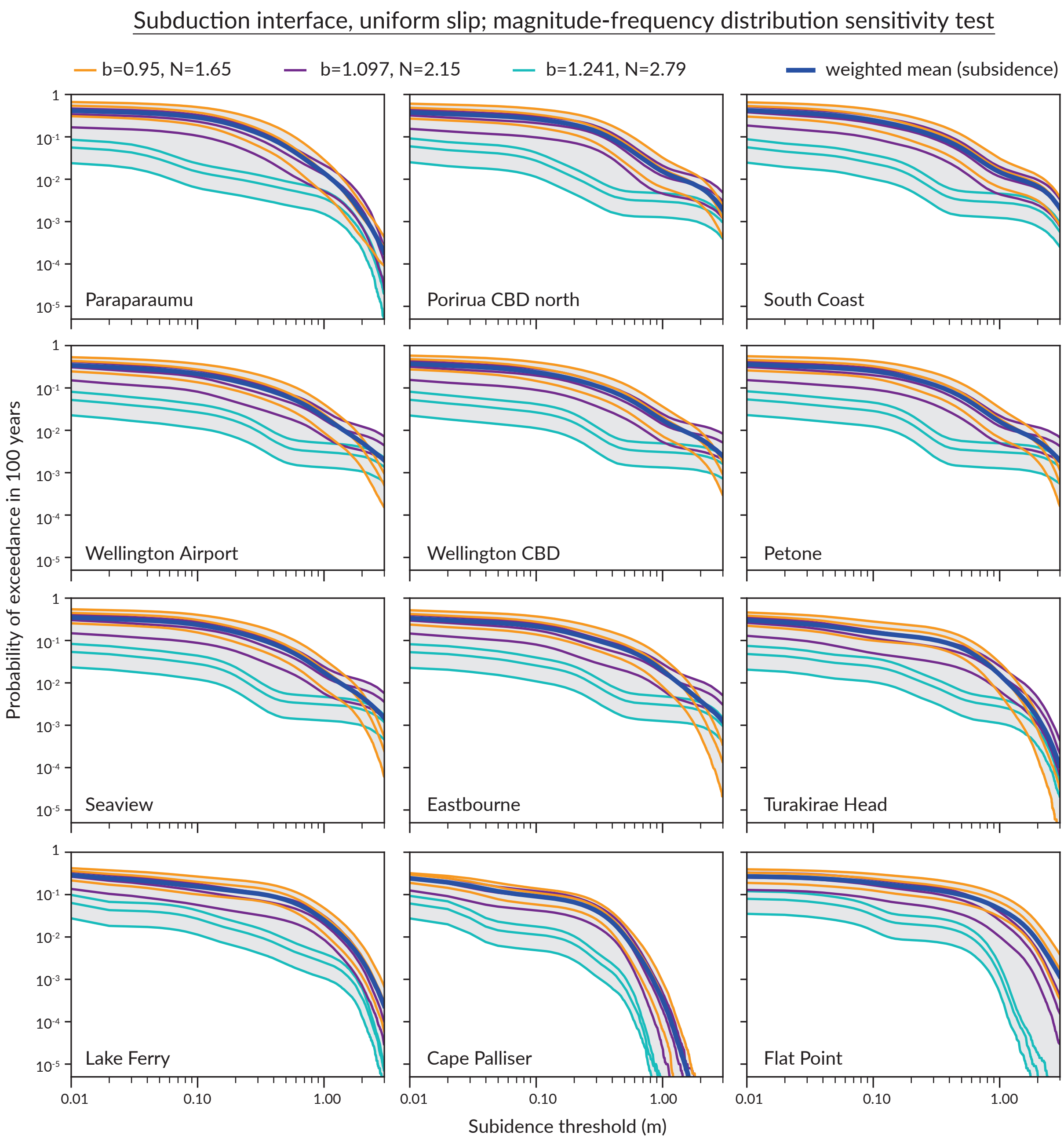

Figure S9: Magnitude frequency distribution parameter sensitivity test for the subduction interface fault moel. Branches with b and N values produce higher probabilities than branches with higher b and N calues. Teal, purple, and orange lines are hazard curves from individual branches and the thick blue line is the weighted mean hazard curve of all branches. Grey dotted and dashed lines are the 10% and 2% probabilities, respectively.

CFM_fault_name	NSHM_fault_sections	CFM_dip_angle_pref	CFM_dip_dir	CFM_rake_pref	model_1_dip_angle	model_1_dip_dir	model_1_rake	model_2_dip_angle	model_2_dip_dir	model_2_rake	rationale
Aotea-Evans Bay	104, 103	70	E	110	70	E	110	50	W	110	might be reverse at depth
Dry River - Huangarua: 1	500, 499, 498, 497, 496, 495	65	NW	90	65	NW	90	30	NW	90	Ninis et al 2023 models
Dry River - Huangarua: 2	501, 502	65	NW	90	65	NW	90	30	NW	90	Ninis et al 2023 models
Dry River - Huangarua: 3	503, 504	65	NW	90	65	NW	90	30	NW	90	Ninis et al 2023 models
Fisherman 1	557, 558	75	NW	90	75	NW	90	75	SE	90	might be backthrusts
Fisherman 2	559, 560, 561	75	NW	90	75	NW	90	75	SE	90	might be backthrusts
Honeycomb	714, 715, 716, 717, 718	40	NW	90	40	NW	90	23	NW	90	accretionary wedge seismic surveys show low angle listric faults
Moonshine	1228, 1227, 1226, 1225	90	subvertical	180	80	SE	-160	80	NW	160	slightly reverse or slightly normal slip
Ohariu	1371, 1370, 1369, 1368, 1367, 1366, 1365,	90	subvertical	180	80	SE	-160	80	NW	160	slightly reverse or slightly normal slip
Ohariu South 1	1372, 1373	65	NW	-135	65	NW	-135	65	NW	160	possibly reverse at depth
Ohariu South 2	1374, 1375	70	NW	-160	70	NW	-160	70	NW	160	possibly reverse at depth
Okupe 1	1401, 1400, 1399, 1398, 1397	75	NW	90	75	NW	90	75	SE	90	might be backthrusts
Opouawe-Uruti	1428, 1429, 1430, 1431, 1432, 1433, 1434, 1435, 1436, 1437, 1438, 1439, 1440, 1441, 1442, 1443, 1444, 1445, 1446	40	NW	90	40	NW	90	23	NW	90	accretionary wedge seismic surveys show low angle listric faults
Otaheke South	1465, 1466, 1467, 1468, 1464	75	NW	135	75	NW	135	75	SE	135	might be backthrusts
Otaki Forks: 1	1469, 1470, 1473	75	NW	160	75	NW	160	75	NW	160	
Otaraia	1486, 1487, 1488, 1489, 1490	60	SE	90	60	SE	90	30	NW	90	Ninis et al 2023 models
Pahaua	1504, 1505, 1506, 1507, 1508, 1509, 1510, 1511, 1512, 1513, 1514, 1515, 1516, 1517, 1518, 1519, 1520, 1521	40	NW	90	40	NW	90	23	NW	90	accretionary wedge seismic surveys show low angle listric faults
Palliser-Kaiwhata	1534, 1533, 1532, 1531, 1530 , 1529, 1528, 1527	40	NW	135	40	NW	135	25	NW	135	Ninis et al 2023 models: need to extend farther south
Pukerua - Shepherds Gully: 1	1601, 1602	90	subvertical	180	80	SE	-160	80	NW	160	try out slightly reverse or slightly normal slip
Pukerua - Shepherds Gully: 2	1603, 1604	90	subvertical	180	80	SE	-160	80	NW	160	try out slightly reverse or slightly normal slip
Pukerua - Shepherds Gully: 3	1607, 1606, 1605	90	subvertical	180	80	SE	-160	80	NW	160	try out slightly reverse or slightly normal slip
Riversdale	1681, 1680, 1679, 1678	40	NW	90	40	NW	90	23	NW	90	accretionary wedge seismic surveys show low angle listric faults
Shephers Gully-Mana	1735, 1736	75	NW	90	75	NW	90	75	SE	90	might be backthrusts
Wairarapa: 1	2098, 2099, 2100, 2101, 2102, 2103	70	NW	160	70	NW	160	55	NW	160	might have small reverse component
Wairarapa: 2	2104, 2105, 2106, 2107, 2108	70	NW	160	70	NW	160	38	NW	160	Ninis et al 2023 models
Wairarapa: Needles	2115, 2114, 2113	70	NW	180	70	NW	180	60	NW	180	slightly gentler dip, but doesn't matter if rake is 180
Wellington Hutt Valley: 1	2199, 2200	70	NW	-160	70	NW	-160	70	NW	-160	Ninis et al 2023 models
Wellington Hutt Valley: 2	2201, 2202	80	NW	160	80	NW	160	75	NW	160	Ninis et al 2023 models
Wellington Hutt Valley: 3	2203, 2204	90	subvertical	180	80	SE	-160	80	NW	160	Ninis et al 2023 models
Wellington Hutt Valley: 4	2207, 2206, 2205	75	SE	-160	75	SE	-160	75	NW	160	Ninis et al 2023 models
Wellington Hutt Valley: 5	2209, 2208	65	SE	-160	65	SE	-160	65	NW	160	
Whareama Bank	2270, 2271, 2272, 2273, 2274, 2275, 2276, 2277, 2278	40	NW	135	40	NW	135	23	NW	135	accretionary wedge seismic surveys show low angle listric faults
Wharekauhau	2279, 2280, 2281, 2282, 2283, 2284, 2285, 2286, 2289	45	NW	90	45	NW	90	31	NW	90	BIG caveat here is that if the wairarapa/wharekauhau merge at depth this is not accounted for.
Whitemans Valley	2320, 2321, 2322	60	NW	110	60	NW	110	45	NW	110	gentler fault at depth based on nearby faults